Relative contributions of synoptic and low-frequency eddies to time-mean atmospheric moisture transport, including the role of atmospheric rivers

Matthew Newman[1], George N. Kiladis[2], Klaus M. Weickmann, F. Martin Ralph[2], and Prashant D. Sardeshmukh[1]

[1]CIRES Climate Diagnostics Center, University of Colorado, and Physical Sciences Division/NOAA Earth System Research Laboratory, Boulder, Colorado

[2]Physical Sciences Division/NOAA Earth System Research Laboratory, Boulder, Colorado

Email: matt.newman@noaa.gov

Submitted to *Journal of Climate*, Saturday, November 12, 2011

ABSTRACT

The relative contributions to mean global atmospheric moisture transport by both the time-mean circulation and by synoptic and low-frequency (periods greater than 10 days) anomalies are evaluated from the mean vertically-integrated atmospheric moisture budget based on 40 years of NCEP-NCAR Reanalysis data. In the extratropics, while the time-mean circulation moves moisture primarily zonally from one part of the ocean to another, low-frequency and synoptic anomalies drive much of the moisture transport both meridionally and from ocean to land. In particular, during the cool season low-frequency variability is the largest contributor to moisture transport into the North American Southwest, Europe, and Australia. While some low-frequency transport originates in low latitudes, much of it is of extratropical origin, due to large-scale atmospheric anomalies that extract moisture from the Northeast Pacific and Atlantic oceans. Low-frequency variability is also integral to the Arctic (latitudes > 70ºN) mean moisture budget, especially during summer when it drives poleward transport from relatively wet high-latitude continental regions. Synoptic variability drives about half of the poleward midlatitude moisture transport in both hemispheres, consistent with simple "lateral mixing" arguments. Atmospheric transport in the extratropics is also particularly focused within "atmospheric rivers" (ARs), relatively narrow poleward-moving plumes of moisture associated with frontal dynamics. AR moisture transport, defined by compositing fluxes over those locations and times where column-integrated water vapor and poleward low-level wind anomalies are both positive, represents most of the extratropical meridional moisture transport. These results suggest that understanding potential anthropogenic changes in the Earth's hydrological cycle may require

understanding corresponding changes in atmospheric variability, especially on low-frequency time scales.

1. Introduction

Perhaps the most striking feature in a satellite loop of the Earth is that the atmosphere transports water across great distances. While this transport appears to occur more frequently in certain regions, it is not steady; rather, it is characterized by numerous transient features of many scales. Thus, to understand atmospheric moisture transport, including the dual role it plays in the global energy cycle and as the source of water over the continents, there is a need to understand how atmospheric variability on different time scales acts to transport moisture and, in turn, is affected by it (e.g. Schneider et al. 2010; Trenberth 2011).

It is well known that transient eddies are a critical part of poleward moisture transport in the extratropics (e.g., Peixoto and Oort 1992). More recently, it has been suggested that virtually all extratropical moisture transport is focused within long, relatively narrow bands sometimes called "atmospheric rivers" (ARs; Zhu and Newell 1998 [hereafter ZN]; Ralph et al. 2004; Neiman et al. 2008a [hereafter N08]). ZN suggested that moisture transport is predominantly confined to these ARs, so that at any given time and at any given latitude about 90% of the meridional moisture transport occurs within only 10% of the zonal band. ARs are particularly striking in column integrated water vapor (IWV) such as is measured by the Special Sensor Microwave Imager (SSM/I), and at times they extend from deep in the Tropics to midlatitudes (Ralph et al. 2011). The extent to which such ARs represent the transport of moisture from the Tropics to the extratropics has been a matter of some debate (e.g., Bao et al. 2006; Knippertz and Wernli 2010), although recent research aircraft observations have confirmed that this can occur (Ralph et al 2011). Studies have shown that the IWV bands

generally are regions of strong surface convergence, and that their leading edges typically correspond to the strong moist low-level jet sometime called the “moist conveyor belt" associated with fronts (Bao et al. 2006; Knippertz and Wernli 2010). Additionally, observational case studies (Ralph et al. 2004; 2005; 2011; Neiman et al. 2008b), composites of many aircraft-observed events (Ralph et al. 2005) and statistical comparison of eight years of reanalysis against SSM/I observations (Ralph et al. 2006; Neiman et al. 2008a) show that the IWV bands can correspond to regions of pronounced moisture flux, i.e., atmospheric rivers.

Two complementary approaches have been used to investigate moisture transport. Given the episodic nature of the IWV bands, it seems natural to use a Lagrangian framework (e.g., Stohl and James 2005; Bao et al. 2006; Eckhardt et al. 2007; Dirmeyer and Brubaker 2007; Knippertz and Wernli 2010; Gimeno et al. 2010; Drumond et al. 2011) and follow the trajectories of individual moist air masses either forward from many different starting locations to determine where the moisture ultimately goes, or backward starting from specified locations and/or precipitation events to find relevant sources. For climate studies the analysis can be computationally expensive, and the trajectory model can be sensitive to errors in the input atmospheric fields as well as errors in the parameterizations and represented dynamics. Also, water vapor is not entirely a passive tracer, so the types of trajectories that can be considered are either limited, especially in their duration, or some assumption must be made to keep track of water phase changes.

For our purposes, it is more straightforward to separate the effects of different time scales of variability in a Eulerian rather than Lagrangian analysis. Eulerian analyses are well suited for determining the relative magnitudes of different processes. Past

Eulerian analyses have generally used global fields generated by state-of-the-art four-dimensional data assimilation systems to evaluate the moisture budget

$$\frac{\partial w}{\partial t} + \nabla \cdot \mathbf{Q} = E - P \,, \tag{1}$$

where w is IWV (also sometimes called "precipitable water"), E is evaporation from the surface, P is precipitation, and $\mathbf{Q}$ is the vertically integrated moisture flux (e.g., Peixoto and Oort 1992). We could determine $\mathbf{Q}$ as a residual from (1) using independent estimates of precipitation and evaporation, including those output by the GCMs used to produce the 'first-guess' fields for data assimilation. However, the atmospheric moisture budget determined from these fields does not balance observed streamflow runoff even on longer time scales (e.g., Betts et al 1999; Lenters et al 2000; Roads and Betts 2000). Alternatively, $\mathbf{Q}$ can be computed using the analyzed wind and humidity fields. This approach has been extensively applied, initially using operational analyses (Trenberth 1991; Roads et al 1994; Trenberth and Guillemot 1995; Wang and Paegle 1996) but more recently using reanalyses (Higgins et al 1996; Mo and Higgins 1996; Higgins et al 1997; Gutowski et al 1997; Min and Schubert 1997; Trenberth and Guillemot 1995; 1998; Betts et al 1999; Roads et al 2002; Mo et al 2005; Schneider et al. 2006; Trenberth et al. 2005; 2007; 2011; Pauluis et al 2011; Shaw and Pauluis 2012; and many others). Globally, and particularly in the extratropics, there is much better agreement amongst different reanalyses for $P - E$ computed as a residual from (1) than for $P - E$ computed from the reanalysis estimates of P and E (e.g., Trenberth et al. 2011). This gives us some confidence in estimates of moisture transport and its divergence as generated from reanalysis humidity and wind fields, and this is the approach we take in this paper.

A few past studies have divided atmospheric moisture transport into contributions from the transient, zonal mean, and stationary portions of the circulation (e.g., Peixoto and Oort 1992; Shaw and Pauluis 2012). On the other hand, most recent studies of variability on "low-frequency" time scales (e.g., intraseasonal to interannual) typically define anomalies as departures from the time averaged atmospheric state, since storm track and climate dynamics in the troposphere are both strongly influenced by zonal and meridional asymmetries of the basic state (e.g., Blackmon et al. 1977; Simmons et al. 1983; Borges and Sardeshmukh 1998; Whitaker and Sardeshmukh 1998; Winkler et al. 2001; Chang et al. 2002). In this study, we investigate the separate contributions of synoptic and low-frequency (LF) anomalies, defined as time-varying departures from the seasonally-varying basic state and split into high (periods < 10 days) and low frequency (periods > 10 days) components, by determining their relative importance to the seasonally-varying climatological mean moisture budget determined from (1). This approach is laid out in section 2 along with a description of the 40-year long dataset. Results are in section 3, where we find that despite the dominance of the mean transport over the oceans, synoptic and LF time scales play critical roles in both meridional and ocean-to-land moisture transport. The contribution of atmospheric rivers to moisture transport is assessed in section 4, and a closer focus on extratropical LF moisture transport is in section 5. Concluding remarks are in section 6.

2. Data and analysis

In sigma coordinates, the vertically integrated moisture flux in (1) is $\mathbf{Q} = \langle q\mathbf{v}p_s \rangle$, where q is specific humidity, p_s is surface pressure, $\mathbf{v}$ is the horizontal wind vector, and brackets

indicate the vertical integral in sigma coordinates, from σ = 1 to σ = 0 (e.g., Trenberth and Guillemot 1995). The vertical integral is most accurately done on the original data levels (Trenberth 1991), which for the dataset used in this paper are sigma coordinates. We define $q = \overline{q} + q' + q''$, and similarly for all other variables, where overbars indicate the seasonally-varying climatological mean, primes (') indicate LF time scale anomalies and double primes (") indicate synoptic time scale anomalies. Anomalies were defined by removing each variable's annual cycle, determined from the first three harmonics of the 4x daily dataset, at each grid point. LF anomalies are determined from a 121-point Lanczos filter that passes periods greater than 10 days, and synoptic anomalies are the residuals representing periods less than 10 days; this frequency cutoff was chosen since it is common to a great many studies of LF variability dating back to Blackmon et al. (1977). Applying these definitions to (1) we obtain the mean moisture budget,

$$\frac{\partial \overline{w}}{\partial t} = -\nabla \cdot \overline{\mathbf{Q}} + (\overline{E} - \overline{P}) \tag{2}$$

where

$$\overline{\mathbf{Q}} = \overline{\langle q \mathbf{v} p_s \rangle} = \langle \overline{q}\,\overline{\mathbf{v}}\,\overline{p_s} \rangle + \langle \overline{p_s}\,\overline{\mathbf{v}'q'} \rangle + \langle \overline{p_s}\,\overline{\mathbf{v}''q''} \rangle \tag{3}$$

or

$$\overline{\mathbf{Q}} = \overline{\mathbf{Q}}^m + \overline{\mathbf{Q}}' + \overline{\mathbf{Q}}''. \tag{4}$$

These terms were computed for each month of the year. [There are also terms missing in (3) depending upon p_s anomalies but these are quite small; for completeness they are included in our computations of $\overline{\mathbf{Q}}'$ and $\overline{\mathbf{Q}}''$.] For the remainder of this paper we label the

terms on the right hand side of (4) the mean transport ($\overline{\mathbf{Q}}^{m}$), LF transport ($\overline{\mathbf{Q}}'$), and synoptic transport ($\overline{\mathbf{Q}}''$). It is important to remember, however, that these are shorthand expressions for moisture transports *by* the mean, *by* LF anomalies, and *by* synoptic anomalies.

The moisture budget was computed for 40 years of NCEP–NCAR reanalysis data covering the period 1968-2007, with wind fields adjusted towards momentum and mass balance using the improved iterative solution of the "χ-problem" (Sardeshmukh 1993) discussed in the Appendix. The budget was also determined from NCEP-DOE Reanalysis 2 data for 1979-2005; for the common period results have only minor quantitative differences so for brevity are not displayed here. All results were smoothed using the Sardeshmukh and Hoskins (1984) spatial filter with n =42 and r = 2.

3. Seasonal variation of the atmospheric moisture budget

a. Winter and summer global moisture transport

Figures 1 and 2 shows the results of (4) for December-February (DJF) and June-August (JJA) 1968-2007. In each figure we show the moisture transport terms $\overline{\mathbf{Q}}^{m}$, $\overline{\mathbf{Q}}'$, and $\overline{\mathbf{Q}}''$ (vectors) and corresponding moisture flux divergences (shading). The upper left panel in each figure shows $\overline{\mathbf{Q}}$ and $\nabla\cdot\overline{\mathbf{Q}}$, the total atmospheric moisture transport and moisture flux divergence; that is, the sum of the three remaining panels. In these two figures $\nabla\cdot\overline{\mathbf{Q}}$ is nearly equal to $\overline{E}-\overline{P}$, since the tendency of the seasonally varying mean w climatology is quite small near the solstices.

The mean transport clearly dominates the total moisture flux (note that the vectors representing both $\overline{\mathbf{Q}}$ and $\overline{\mathbf{Q}}^m$ are scaled by a factor of 10 larger than for the other two terms). This is also true for the transition seasons (not shown). The gross features of the mean transport are familiar from other studies, showing broad areas of moisture sources (positive $\overline{E} - \overline{P}$) within the subtropics, and sinks over the continents, the midlatitude storm tracks, and the warm pool and monsoon regions of the Tropics. Mean transport during DJF in the Northern Hemisphere is mostly zonal and only somewhat poleward, from the western to the eastern margins of the North Pacific and North Atlantic Ocean basins. There is also strong zonal transport in the Southern Hemisphere extratropics, but it is sufficiently uniform that its associated moisture divergence is relatively small. Extratropical zonal transport is stronger in both hemispheres during DJF than JJA. The net transport by winds swirling around the mean subtropical highs in the summer hemispheres is primarily westward but there is also some higher latitude poleward transport.

Figures 1 and 2 might give a somewhat misleading picture of the water cycle, because a large fraction of the atmospheric moisture transport essentially moves water zonally from one part of the ocean to another (which does have important implications for ocean dynamics by changing surface salinity; see, for example, Huang 1993; Delcroix et al. 1996). While this "ocean-to-ocean" moisture transport is dominated by the mean transport, both ocean-to-land transport and meridional transport are not, which can initially be seen by close inspection of Figs. 1 and 2. Also, even though the synoptic and LF transports are generally much weaker than the mean transport, their corresponding flux divergences are comparable in many regions (note that in Figs. 1 and 2 the contour

interval of flux divergence is the same in all panels) so that anomaly moisture transport is important to the overall moisture budget.

b. Ocean-to-land moisture transport

The importance of the LF and synoptic terms for ocean-to-land moisture transport is shown in Figs. 3a-e, which displays the inflow of moisture into several different land regions (determined from the areal average of each corresponding moisture convergence term within each region) as a function of the seasonal cycle. In the global average (not shown), the mean, LF, and synoptic transports drive about 77%, 12%, and 11%, respectively, of annual mean ocean-to-land transport. This result, however, is dominated by the Tropics (Fig. 3a) where the mean trades transport moisture from the ocean into the tropical convergence zones including those over land, with LF anomalies (and, to a lesser extent, synoptic anomalies) acting to transport some moisture out of the convergence zones back to the ocean. On the other hand, for annual mean extratropical ocean-to-land transport the three terms have roughly equal importance, since during the cool season moisture is mainly transported by both $\overline{\mathbf{Q}}'$ and $\overline{\mathbf{Q}}''$ (see Figs. 3b and c), more than offsetting the usually dominant role of $\overline{\mathbf{Q}}^m$ during summer (e.g., JJA in the Northern Hemisphere and DJF in the Southern Hemisphere).

During DJF, the pattern of LF transport is very different from that of synoptic transport, and the corresponding "source" regions are also different (cf. Figs. 1c and d). Notably, LF source regions in the eastern extratropical Atlantic and Pacific exist that export moisture, both eastward and westward as well as poleward. Although LF transport might seem small in Figs. 1 and 2, it nonetheless is the difference between a moisture

deficit and surplus in key areas such as the North American southwest and Europe (Fig. 3e) in DJF, and southern Australia and New Zealand in JJA, especially since in all these areas the mean flow acts to remove moisture. Averaged over the entire North American continent, synoptic transport is slightly larger than LF transport (Fig. 3d); but the relative importance of these two terms varies between the western half of North America, where LF transport from sources in both the extratropical and subtropical east Pacific is greater (more so for the northwest and southwest, respectively), and the eastern half of North America, where synoptic transport is greater. For Europe, both the Atlantic and Mediterranean act as LF sources (see also Gimeno et al. 2010). Note also that both LF and synoptic transports substantially broaden the moisture sinks on the poleward sides of the subtropical highs during JJA.

c. Meridional moisture transport

The well-known importance of transients in driving meridional moisture transport (e.g., Oort and Peixoto 1992) is evident in Fig. 4, which shows the zonal average of each term contributing to the total Q^y, the meridional component of **Q**, as a function of the seasonal cycle (Figs. 4a-d) and for the annual mean (Fig. 4e). In the tropics and subtropics, the mean circulation dominates meridional transport, and this is primarily equatorward but with a cross-equatorial component towards the summer hemisphere near the solstices (see also Schneider et al. 2006). In the extratropics the synoptic transport is the largest term, especially in the Southern hemisphere. As we might expect, synoptic transport is largest within the storm tracks over the western part of both Northern hemisphere ocean basins (Fig. 1d) where synoptic variability is strongest (e.g., Chang et al. 2002; see also Fig. 11b, below), with the maxima moving poleward with the storm tracks in summer (Fig.

2d). Note that the moisture source for synoptic transport lies poleward of the mean transport source (cf. Figs. 1b and 1d). Also, synoptic transport is almost entirely meridional, with its small zonal component making little contribution to the flux divergence. Meridional LF transport is only about half the amplitude of the synoptic transport but acts over a broader latitude range, and has a somewhat greater effect in the Pacific sector (not shown, but see Figs. 1c and 2c) than for the zonal mean.

Moisture transport into the polar regions can be determined by the value of the zonally averaged meridional transport at 70º N and S in Fig. 4. Total transport into the Arctic (Fig. 3f) peaks during summer, in agreement with earlier studies (e.g., Serreze et al. 2006; 2007). LF anomalies drive close to two thirds of this transport every month of the year. In the winter the LF transport occurs primarily over the Atlantic, but in the summer it is dominated by poleward transport from the large land masses toward the Arctic ocean (cf. Figs. 1c and 2c). Much of this transport occurs from Eurasia, consistent with an increased frequency of blocking there during summer (e.g., Tyrlis and Hoskins 2008; Dole et al. 2011) as well as a pronounced summertime maximum over northern Eurasia in w' variance (not shown). We find that LF moisture anomalies are in phase with LF meridional wind anomalies related to blocks (not shown), consistent with poleward moisture transport occurring as southerlies (northerlies) to the west (east) of the block transport anomalously moist (dry) air from the continent (polar region). In contrast, synoptic and LF transports into the Antarctic are about equally important (not shown), and these have spring and fall maxima, consistent with the Southern Hemisphere semi-annual oscillation (van Loon 1967).

d. Analysis of transport terms

It is instructive to separate moisture flux divergence $\nabla \cdot \mathbf{Q}$ into the moisture advection and divergence terms, $\langle \mathbf{v} \cdot \nabla(qp_s) \rangle$ and $\langle qp_s \nabla \cdot \mathbf{v} \rangle$, respectively, computed separately from the mean and from LF and synoptic anomalies, shown in Fig. 5 for DJF. Note that both terms represent vertically integrated quantities. So, for example, to the west (east) of the Rockies, $\langle \overline{\bar{q}\bar{p}_s} \nabla \cdot \bar{\mathbf{v}} \rangle$ generates a net moisture sink (source) due to mean rising (subsiding) motion since there is much more atmospheric moisture at lower levels than at upper levels. In the extratropics, strong mean zonal flow advects continental dry air over the warm western boundary currents, which act as moisture sources for the atmosphere. In the central and northeastern extratropical ocean basins, moisture sinks are balanced by both northeastward advection of moist air over increasingly cooler oceans and particularly into much drier continents, and by strong moisture convergence due to deceleration of the winds in the jet exit region. In the storm tracks, where rising (subsiding) motion generally occurs in anomalously wet (dry) regions, the convergence term acts as a synoptic moisture sink, while the advection term serves primarily as the synoptic moisture source. In contrast, LF moisture sources and sinks are driven almost entirely by advection alone since the convergence term is negligible, consistent with the more barotropic nature of large-scale LF anomalies.

The time scale dependence of LF transport is examined by applying additional time filters. As in section 2, we define $q' = q^{10\text{-}30} + q^{30\text{-}90} + q^{90+}$, and similarly for all other variables, where the superscripts represent the bandpass interval (in days) determined from additional applications of the Lanczos filter, with 90+ representing a filter that passes all periods longer than 90 days. The relative importance of different bands during

DJF varies strongly by location, as shown in Fig. 6. Transport by the 10-30 day band represents more than half the LF transport into the eastern half of North America but under one third over the North Atlantic and Europe, where longer time scale (>90 days) anomalies drive almost half. The strongest moisture convergence occurs in the 10-30 day band along the eastern, southern and western boundaries of the Continental US, associated with strong northward or northeastward transports. Most of the LF transport in the Southern Hemisphere is in the 10-30 day band, with the notable exception of south Australia. However, the transport out of the SPCZ gains an additional eastward component with increasing time scale, so that its moisture flux divergence is about the same for each band (this occurs year-round; not shown).

4. Impact of "atmospheric rivers" on the atmospheric moisture transport

The statistical analysis described in the preceding section, of course, yields a picture that is representative of the net effect of all individual events. In this section we examine this more closely, also considering the impact of "atmospheric rivers" as described, for example, by ZN and N08. As an example, Fig. 7 shows a time-longitude diagram of the 4 times daily **Q** and w at 35ºN (left) and 45ºN (right) for DJF 2003 and 2004. For comparison, Fig. 8 repeats the left panels of Fig. 7 but uses data in which either the synoptic components or the LF components are removed before **Q** and w are computed. Even over these relatively short periods, we can see elements of the different time scales for transport shown in Fig. 1. In the central Pacific, moisture transport is clearly dominated by synoptic events, with pronounced poleward transport occurring in fairly

narrow bands that occur with some regularity and that propagate rapidly eastward. There is almost no corresponding equatorward transport, and in particular there appears to be almost no poleward moisture transport that results from dry air advected equatorward. On the other hand, near the midlatitude coasts (around 120ºW and 5ºW), the LF transport component is more evident with much longer periods of strong and weak transport, especially inland, and even some instances of equatorward transport (see also Fig. 8). At higher latitudes in both ocean basins the transport almost always occurs within a fairly narrow longitude range and is much more persistent overall.

Because at any given time much of the transport is located within fairly narrow spatial bands, ZN suggested that the bands represent "atmospheric rivers", which they defined as filament-like structures of moisture flux representing most of the global total moisture transport. They categorized these regions by finding all locations where the magnitude of $\mathbf{Q}$, $|\mathbf{Q}|$, was relatively higher than its zonal mean value. Specifically, their algorithm determined that a river existed wherever and whenever $|\mathbf{Q}| \geq |\mathbf{Q}_{mean}| + 0.3(|\mathbf{Q}_{max}|-|\mathbf{Q}_{mean}|)$, where $\mathbf{Q}_{mean}$ is the zonal mean $\mathbf{Q}$ and $\mathbf{Q}_{max}$ is the longitudinal maximum, both of which are functions of latitude and time.

To gain a comprehensive picture of the effect of ARs on atmospheric moisture transport, we composited $\mathbf{Q}$ in those regions and times in our 40-year dataset where AR conditions occur, using the ZN definition, and also determined the frequency of AR condition occurrence worldwide. The results (Fig. 9a) confirm that, as ZN suggested from much more limited data, the flux associated with atmospheric rivers defined in this way represents a large portion of the total moisture flux field, and virtually all of the extratropical meridional transport. On the other hand, comparison of Fig. 9d to Fig. 1a

shows that the AR composite takes into account neither transport by the mean subtropical highs in the Southern Hemisphere (and similarly for the Northern Hemisphere during summer, not shown) nor the substantial zonal transport that remains in the extratropical jets of both hemispheres. Additionally, the ZN split of tropical transport seems potentially artificial.

One concern regarding the ZN definition is that it is somewhat ad hoc, since there is no precise justification for its form; in fact, ZN determined the threshold value 0.3 because it gave the "best" fit to the total moisture flux field computed from the data for one day, 12 October 1991. Changing the threshold parameter gives quite different results: if it is weakened (0.1) then almost all moisture flux worldwide is categorized as "AR" flux and in the NE Atlantic AR conditions occur more than 75% of the time, whereas if it is strengthened (0.5) then the frequency of AR events is so reduced that the AR composite explains only about half of the total flux in the North Pacific. Additionally, the ZN definition does not differentiate between transient and steady moisture transport. The mere fact that moisture transport is much stronger over the oceans than over land, as is the case for transport by the mean circulation in the extratropics (cf. Fig. 1b), is enough to cause many regions to nearly continuously reach the AR threshold, most obviously in the North Atlantic. In fact, all the regions in Fig. 9a where the AR conditions occur at least 20% of the time are also regions where the transport by the mean alone passes ZN's AR test. This sensitivity to an arbitrary parameter complicates any diagnosis of how ARs contribute to the total moisture transport.

Note from Fig. 7 that moisture flux is typically strongest in regions where moisture anomalies are large. This relationship between moisture and moisture flux is

fairly general in the extratropics: polewards of about 30º, the correlation between w and $|\mathbf{Q}|$ is ~0.7-0.85 during DJF (DJF/JJA) in the Northern (Southern) Hemisphere and ~0.5-0.75 during JJA in the Northern Hemisphere (not shown) over the entire 4 times daily dataset. This correlation supports the approach taken in past AR studies to use IWV as a proxy for **Q** (Ralph et al. 2004, 2005, 2011; Neiman et al, 2008a, 2008b). In these studies, which were focused on determining ARs in midlatitudes (often using SSM/I data), ARs were defined using both a threshold value for w of 2 cm and a key spatial pattern requirement which retained only narrow plumes that were >2000 km long and <1000 km wide. We defined a somewhat similar criterion by adapting the ZN approach to w, specifying that rivers exist wherever $w \geq 2$ cm and additionally that $w \geq w_{mean} + 0.3(w_{max} - w_{mean})$ on a latitude circle, but with no other shape criterion, and then applied this definition to the entire dataset to produce the results shown in Fig. 9b and e. Clearly, this AR definition is useful for some areas including the west coast of the U.S., but it is not general enough for worldwide extratropical application, particularly at much higher latitudes in the Pacific and Atlantic oceans where typical values of w are less than 2 cm yet strong winds still yield pronounced moisture fluxes. On the other hand, it is interesting to note that all wintertime land-falling AR events that N08 identified from their 8-yr dataset are associated with large moisture and flux LF anomalies reaching the coast (e.g., left panels of Fig. 8).

An important aspect of the above criteria is that the AR region is defined as relatively narrow, which introduces an element of subjectivity into the definition; namely, how narrow is narrow enough? Also, as noted by Bao et al. (2006), ARs are generally coincident with strong surface convergence, so when the narrowness of the region is

associated with frontal dynamics it may not be a necessary condition. Nevertheless, these definitions capture the essence of extratropical moisture transport as is seen in Fig. 7, since they identify plumes of moisture with regions of intense poleward moisture transport, as in Ralph et al. (2004). This leads us to examine categorizing "AR" conditions as the occurrence of episodic poleward moving moisture plumes, without requiring a shape requirement. Fig. 9c shows the results obtained by compositing over all times/locations for which the 4 times daily (unfiltered) w and poleward low-level meridional v_{low} wind *anomalies* are both positive; here, v_{low} is defined as the meridional wind vertically integrated between the surface and σ=0.85, although results are insensitive to the integral's upper bound. It is striking that the extratropical results are so similar to Figs. 9a and 9b; in fact, the composite poleward moisture flux is even greater than the mean. Fluxes in the three remaining groupings (w and $v_{low} < 0$, $w > 0$ and $v_{low} < 0$, $w < 0$ and $v_{low} > 0$) are each weaker, and contribute roughly equally to the remaining zonal flux in the extratropics, with a somewhat larger equatorward component from the w and $v_{low} < 0$ grouping (not shown).

The composite in Fig. 9c shows that extratropical moisture transport is associated primarily with anomalous poleward advection of positive moisture anomalies. At any given time, then, ARs are indeed those regions where most of the extratropical moisture flux is located. It is also interesting that the variances of both moisture and meridional wind synoptic anomalies (shown for wintertime in Fig. 10) lie within the region of strongest climatological meridional moisture gradient, with mean moisture relatively well mixed both to the north and south (see the top panel of Fig. 10). Since synoptic moisture transport is predominantly meridional, the AR composite suggests a simple "lateral

mixing" argument for the moisture flux (illustrated in Fig. 11a): anomalous poleward wind generates a positive moisture anomaly (a "plume") that transports moisture poleward, but at the same latitude anomalous equatorward wind does not generate a negative moisture anomaly so it does not contribute to the transport. This is essentially the converse of the argument Pierrehumbert (1998) makes for the transport of dry extratropical air into the subtropics, so we have appropriated his term to describe the process. Thus, a simple scaling analysis for extratropical moisture transport is $\mathbf{Q} \approx Q^y \sim v\Delta w$, where Δw is the difference (decrease) in precipitable water from the Tropics to the extratropics within the storm track region (as illustrated in Fig. 11a). From Fig. 10, typical values in the Pacific are $v''_{low} \sim 5$ m/s and $\Delta w \sim 10$ mm, yielding $w'' \sim 10$ mm and $Q^y \sim 50$ kgm^{-1}s^{-1}, both consistent with observations.

This picture can be somewhat generalized in two ways. First, note that the maximum in v''_{low} amplitude should coincide with the zero line of moisture flux divergence: v''_{low} increases (decreases) as air south (north) of the v''_{low} maximum moves poleward so that Q^y must also increase (decrease) with latitude, resulting in moisture divergence (convergence) and hence a moisture source (sink). This is consistent with the synoptic advection term in Fig. 5; also, enhanced evaporation is proportional to surface wind anomalies (e.g., Alexander and Scott 1997). Second, as the moisture plumes are advected poleward, they are simultaneously advected by the time mean flow (as in Fig. 7) so that they do not represent strictly meridional transport. Thus, *the AR composite does not simply resemble the synoptic transport but also contains much of the mean transport*. It follows that when a moisture plume is not present, advection due to the strong zonal winds should be much less. Note that this simple picture is still incomplete since we have

not considered the synoptic moisture sink due to the divergence term (Fig. 5), that is, due to low-level convergence and rising motion (e.g., into the "moist conveyor belt"; Bao et al. 2006) leading to precipitation.

5. LF transport over the wintertime extratropical oceans

The lateral mixing argument of the previous section does not appear to be consistent with the observed variability of LF moisture and circulation anomalies, also shown in Fig. 10, or their associated moisture transport. Most of the extratropical meridional wind variability on LF time scales, associated with changes in local zonal jets and storm tracks, is located in the northeastern portions of the Atlantic and Pacific basins, away from regions of strong mean moisture gradient. Yet as seen in Fig. 5, LF moisture flux divergence is predominantly associated with the advection term. This suggests that a process connected to the typical large-scale LF anomalies of both the Pacific and Atlantic basins must be driving extratropical LF transport. For example, over the Pacific a common LF anomaly involves a strengthening or weakening of the Aleutian low with corresponding wind anomalies, as illustrated in Fig. 11b. Changes in the surface zonal winds (red lines) will also change surface evaporation (Cayan 1992; Alexander and Scott 1997), and meridional wind anomalies will advect dry air anomalies equatorward and moist air anomalies poleward. This gives rise to moisture flux that is both northwestward and northeastward from the source region, with the anomalous moisture gradient in the same direction as the wind anomaly as in Fig. 11b. Note that a LF anomaly of either sign will lead to the same pattern of moisture transport, so on *average* this anomaly will contribute to mean transport.

To see if this effect exists in nature, we first computed the principal components (PCs) of u'_{low} (LF zonal wind anomaly integrated from the surface to $\sigma = 0.85$) during winter over either the Pacific sector (120ºE-120ºW) or the Atlantic sector (90ºW-0º) in the Northern Hemisphere. The global fields of u'_{low}, v'_{low}, and w' are then regressed on the leading Pacific PC, PC1/PAC (Fig. 12a) and also on the leading Atlantic PC, PC1/ATL (Fig. 12c). In both basins, anomalous surface westerlies (easterlies) are indeed associated with an anomalous positive (negative) zonal gradient of moisture LF anomalies. For example, from Fig. 12a, at about 30ºN, 150ºW the regressed wind speed is about 0.8 ms^{-1} and the moisture gradient is about .0025 mm/km, so that the flux convergence is about .17 mm/day. This estimate does not take into account the vertical profiles of winds or moisture, so it probably underestimates the total flux. Alternatively, in Fig. 12b we show the composite of $\overline{\mathbf{Q}}'$ and its associated divergence for all high amplitude PC1/PAC events of *both* signs, that is, when the amplitude of PC1/PAC was either greater than +2 standard deviations or less than -2 standard deviations. The result is again consistent with the simpler argument outlined in Fig. 11b. In particular, the individual composites based on $+2\sigma$ PC1/PAC and -2σ PC1/PAC (not shown) both have similar, statistically significant patterns of flux and flux divergence, with the same sign, except that the convergence near 165ºE is only associated with an anticyclonic anomaly. The corresponding composite for the PC1/ATL is shown in Fig. 12d. In this case, although the individual composites again have similar patterns, the $+2\sigma$ composite amplitude is much larger.

Previous studies (Cayan 1992; Alexander and Scott 1997) have identified the northeast Pacific and Atlantic as regions of strong latent heat flux exchange between the

ocean and atmosphere on LF time scales, and this flux is strong enough to drive much of the North Pacific SST anomaly associated with ENSO (Alexander et al. 2002). The net energy flux associated with the North Pacific moisture source in Fig. 1c is $L(E\text{-}P)$, which for L =2.5 x 10^6 J/kg and $E\text{-}P$ ~ 1.7 mm/day is ~ 50 W/m^2. In comparison, the total 1968-2006 DJF mean latent heat flux in this location (35ºN, 142ºW) from the OAflux dataset (Yu et al. 2008) is about 85 W/m^2. It is also interesting to note that a local ridge in the DJF mean latent heat flux field from OAflux (not shown) is centered along a line that extends from about (22ºN, 147ºW) to (46ºN, 130ºW), which is coincident with the maximum in $\nabla \cdot \overline{\mathbf{Q}}'$.

6. Concluding remarks

Although there have been many previous analyses of the atmospheric moisture budget, including those that have demonstrated the importance of transient eddies to meridional moisture transport, it has not been previously shown how synoptic versus LF time scales impact climatological moisture transport. An analysis of the seasonal cycle of the mean vertically integrated atmospheric moisture budget using 40 years of NCEP-NCAR Reanalysis data reveals that during the cool season in the extratropics of both hemispheres, LF and synoptic anomalies play a significant role in the atmospheric transport of moisture from ocean to land. This occurs despite the fact that the mean transport generally has much larger amplitude, because much of the mean transport does not move moisture onto land so much as move moisture zonally from the western to the eastern margins of the ocean basins. In some regions, such as the North American Southwest, Europe, and Australia, LF transport is the largest contributor to wintertime

and even annual mean atmospheric moisture. LF transport is also critical to the Arctic moisture budget throughout the year and reaches maximum amplitude during summer, associated with moisture transport from land to ocean especially over Eurasia.

In addition, it is striking how the patterns of LF and synoptic transports differ from each other. Despite its relatively small impact in a global sense, LF transport is a key moisture source for continental precipitation during winter. Note that while the sources associated with synoptic transport are fairly similar to the dominant global mean moisture sources, LF transport sources are not, and in fact in many areas oppose the mean. This suggests that it may be of interest to consider these regions as starting points for Lagrangian analyses, especially for case studies of moisture source regions connected to LF variability.

This paper has also examined the potential role of atmospheric rivers in the global water budget and explored a method to systematically diagnose AR contributions to moisture transport without necessarily including a dependence on width and length (e.g., large values of IWV in long and narrow regions in the extratropics) used in recent diagnostic studies by Ralph et al. and Neiman et al. The results verify that ARs are the primary regions where extratropical atmospheric moisture transport occurs. An individual AR event is the sum of its mean, synoptic, and LF components. AR moisture transport over the northern midlatitude oceans then essentially consists of poleward and eastward advection of a moisture plume originating within subtropical source regions, plus additional moisture extracted from the ocean in the western storm track region by synoptic scale meridional winds, plus moisture extracted in the northeast part of the basin depending on the state of the LF anomaly (e.g., an intensification of the Aleutian low),

minus the water precipitated out polewards of the storm track across the ocean. In this view, ARs do not simply represent *trajectories* of moisture transport from the Tropics/subtropics since on average ARs also pick up additional moisture as they cross the oceans, a point similar to one made in case studies of some AR events by Bao et al. (2006).

It has been shown that on at least a few occasions some moisture may be transported directly from the tropics within ARs (Bao et al. 2006; Stohl et al. 2008; Ralph et al 2011). In fact, a moisture source for North America due to LF variability exists in the eastern tropical Pacific, although it may be more relevant for Mexico than regions farther north. But we also find a mechanism with perhaps greater impact that represents at most only an *indirect* effect of the Tropics on extratropical moisture and its transport. During wintertime, ENSO is well known to cool (warm) the North Pacific sea surface by intensifying (weakening) the Aleutian low leading to enhanced (weakened) latent heat flux (the "atmospheric bridge"; Alexander et al. 2002). Our results suggest that during this process moisture is extracted from the sea surface for LF anomalies of either sign, with much of this moisture then transported toward western North America. That is, tropical forcing may produce circulation anomalies that transport additional moisture from an extratropical source while not actually transporting moisture all the way from the Tropics. Note that extratropical LF variability of this type can also occur without tropical forcing (e.g., Winkler et al. 2001), and that details of the tropical forcing may influence the extratropical LF anomalies (e.g., Winkler et al. 2001; Di Lorenzo et al. 2010) and how they interact with the sea surface. Whether this process is likewise important to moisture transported by individual synoptic and LF events, including those ARs that give

the appearance of direct transport of moisture from the Tropics, is the subject of our current research.

Finally, we note that changes in the hydrological cycle are also fundamental to anthropogenic climate change scenarios, impacting precipitation patterns (e.g., Trenberth 2011), large-scale circulation (Held and Soden 2006) and driving much of the global "warming" itself (e.g., IPCC 2007; Compo and Sardeshmukh 2009). Our results, and particularly the importance of LF atmospheric variability for transporting moisture into extratropical land masses, suggests that understanding potential anthropogenic changes in the Earth's hydrological cycle may require understanding corresponding changes in atmospheric variability, especially on low-frequency time scales.

7. Acknowledgments

The authors wish to thank Jim Adams for drafting Figure 11, and Gary Wick for assistance with the SSM/I data.

8. Appendix

There are many potential sources of error in computing (1) from analyzed datasets, but perhaps the most important is the notable difference in the divergent wind field between reanalyses. This is particularly true in the Tropics (Newman et al. 2000), but can even be true in the extratropics such as for the low level jet (LLJ), which transports a significant fraction of moisture during summer (e.g., Helfand and Schubert 1995). Thus, the most important correction to **Q** can be made by improving the wind analysis (Trenberth and Guillemot 1995; Wang and Paegle 1996; Min and Schubert 1997; Mo and Higgins 1998). Specific humidity corrections on the order of 3% have also been made but these have

typically been applied only to the mean field (Large and Yeager 2009). For daily-averaged values, we find that for the years 1997-2007 over the oceans *w* from reanalysis and IWV from SSM/I are generally well correlated (0.8-0.95) throughout the extratropics and less well (0.5-0.7) in the Tropics, although since tropical moisture variance is much less it might be more susceptible to small errors (cf. Fig. 10a).

How can we get a better estimate of the wind field? One approach is to note that t-he error in the analyzed wind fields is predominantly in the divergent component of the wind, and less so for the rotational component, consistent with the fact that the large-scale vorticity analyses produced at different data centers are in much better agreement than the corresponding divergence analyses (e.g., Newman et al 2000). One way to correct the analyzed divergence is by constraining the winds to minimize imbalances in both the mass and vorticity budgets, thus enforcing dynamical consistency upon the divergent circulation. This approach, known as the 'chi-problem' (Sardeshmukh 1993), has been successfully used to correct tropical divergence fields (Sardeshmukh and Liebmann 1993; Sardeshmukh et al 1999), but the approach is applicable globally. A long-term global heating dataset developed using the 'chi-corrected' horizontal wind and vertical velocity fields, where heating is then estimated as a residual in the heat budget, has been used for studies of short-term climate variability in and related to the Tropics (Winkler et al. 2001; Lin et al. 2004; Newman and Sardeshmukh 2008; Newman et al. 2009), since we have found that this technique yields improved diabatic heating estimates (Sardeshmukh et al 1999). It can similarly improve moisture flux estimates. Fig. A1a shows that in the Tropics, the chi-corrected vertical profile of the November-February 1992-93 mean "moisture sink" (Q2, Yanai et al. 1973) compares better with TOGA-

COARE observations (Johnson and Ciesielski 2000) than does the same quantity computed from the NCEP Reanalysis. The chi-correction also acts to slightly lower the low level jet altitude over the central United States, as shown in Fig. A1b for July 1993. A similar change is evident during June-August 1994 (not shown), which is consistent with profiler data showing the jet centered about 50 mb lower than in reanalysis data (Higgins et al 1997). The chi-correction is a conservative adjustment to the winds, well within the observational margin of error. Yet, during the warm season, a slightly stronger and lower chi-corrected low level jet results in a larger estimate of *P-E* in the Great Plains (Fig. A1c), consistent with earlier work suggesting a large dry bias in the reanalysis in the warm season over North America (e.g., Mo and Higgins 1996; Yeh et al 1998; Roads and Betts 2000; Lenters et al 2000).

9. References

Alexander, M. A., and J. D. Scott, 1997: Surface flux variability over the North Pacific and North Atlantic oceans. *J. Climate*, **10**, 2963–2978.

Alexander, M. A., I. Bladé, M. Newman, J. R. Lanzante, N.-C. Lau, and J. D. Scott, 2002: The atmospheric bridge: the influence of ENSO teleconnections on air-sea interaction over the global oceans. *J. Climate*, **15**, 2205-2231.

Bao, J.-W., S. A. Michelson, P.J. Neiman, F. M. Ralph and J. M. Wilczak, 2006: Interpretation of enhanced integrated water vapor bands associated with extratropical cyclones: Their formation and connection to tropical moisture. *Mon. Wea. Rev.*, **134**, 1063-1080, doi:10.1175/MWR3123.1.

Betts, A. K., J. H. Ball, and P. Viterbo, 1999: Basin-scale surface water and energy budgets for the Mississippi from the ECMWF reanalysis. *J. Geophy. Res.*, **104**, 19293-19306.

Blackmon, M. L., J. M. Wallace, N.-C. Lau, S. L. Mullen, 1977: An Observational Study of the Northern Hemisphere Wintertime Circulation. *J. Atmos. Sci.*, **34**, 1040–1053.

Borges, M. D., and P. D. Sardeshmukh, 1995: Barotropic Rossby wave dynamics of zonally varying upper level flows during northern winter. *J. Atmos. Sci.,* **52,** 3779–3796.

Cayan, D.R., 1992: Latent and sensible heat flux anomalies over the northern oceans: the connection to monthly atmospheric circulation. *J. Climate*, **5**, 354-369.

Chang, E. K. M., S. Lee, and and K. L. Swanson, 2002: Storm Track Dynamics. *J. Climate*, **15**, 2163–2183.

Compo, G. P., and P. D. Sardeshmukh, 2009: Oceanic Influences on Recent Continental Warming. *Clim. Dyn*., **32**, 333–342. DOI:10.1007/s00382-008-0448-9.

Delcroix T., C. Henin, V. Porte, and P. Arkin, 1996: Precipitation and sea-surface salinity in the tropical Pacific Ocean. *Deep Sea Res Part I*, **43**, 1123–1141. doi:10.1016/0967-0637 (96)00048-9.

Di Lorenzo, E., K. M. Cobb, J. Furtado, N. Schneider, B. Anderson, A. Bracco, M. A. Alexander, and D. Vimont, 2010: Central Pacific El Niño and decadal climate change in the North Pacific. *Nature Geosciences*, 3 (11), 762-765, doi: 10.1038/NGEO984.

Dirmeyer, P. A., K. L. Brubaker, 2007: Characterization of the Global Hydrologic Cycle from a Back-Trajectory Analysis of Atmospheric Water Vapor. *J. Hydrometeor*, **8**, 20–37.

Dole, R., M. Hoerling, J. Perlwitz, J. Eischeid, P. Pegion, T. Zhang, X.-W. Quan, T. Xu, and D. Murray, 2011: Was there a basis for anticipating the 2010 Russian heat wave? *Geophys. Res. Lett*., **38**, L06702, doi:10.1029/2010GL046582.

Drumond, A., R. Nieto, and L. Gimeno, 2011: On the contribution of the Tropical Western Hemisphere Warm Pool source of moisture to the Northern Hemisphere precipitation through a Lagrangian approach, *J. Geophys. Res*., **116**, D00Q04, doi:10.1029/2010JD015397.

Eckhardt, S., A. Stohl, H. Wernli, P. James, C. Forster, N. Spichtinger, 2004: A 15-Year Climatology of Warm Conveyor Belts. *J. Climate*, **17**, 218–237.

Gimeno, L., A. Drummond, R. Nieto, R. M. Trigo, and A. Stohl, 2010: On the origin of continental precipitation. *Geophys. Res. Lett.*, **37**, L13804, doi:10.1029/2010GL043712.

Gutowski, W. J., Y. Chen, and Z. Otles, 1997: Atmospheric water vapor transport in NCEP-NCAR reanalyses: Comparison with river discharge in the central United States. *Bull. Amer. Meteor. Soc.*, **78**, 1957- 1969.

Helfand, H. M., and S. D. Schubert, 1995: Climatology of the simulated Great Plains low-level jet and its contribution to the continental moisture budget of the United States. *J. Climate*, **8**, 784-806.

Held, I. M., and B. J. Soden, 2006: Robust responses of the hydrological cycle to global warming. *J. Clim.*, **19**, 5686-5699.

Higgins, R. W., K. C. Mo, and S. D. Schubert, 1996: The moisture budget of the central United States in Spring as evaluated in the NCEP/NCAR and the NASA/DAO reanalyses. *Mon. Wea. Rev.*, **124**, 939- 963.

Higgins, R. W., Y. Yao, E. S. Yarosh, J. E. Janowiak, and K. C. Mo, 1997: Influence of the Great Plains low-level jet on summertime precipitation and moisture transport over the central United States. *J. Climate*, **10**, 481-507.

Huang, R. X., 1993: Real Freshwater Flux as a Natural Boundary Condition for the Salinity Balance and Thermohaline Circulation Forced by Evaporation and Precipitation. *J. Phys. Oceanogr.*, **23**, 2428–2446.

IPCC (Intergovernmental Panel on Climate Change) 2007: Climate change 2007. The physical science basis. Solomon Q, Qin D, Manning M, Chen Z and others (eds) Contribution of Working Group 1 to the 4th assessment report of the Intergovernmental Panel on Climate Change. Cambridge University Press, Cambridge

Johnson, R.H., and P.E. Ciesielski, 2000: Rainfall and Radiative Heating Rate Estimates from TOGA-COARE Atmospheric Budgets. *J. Atmos. Sci*. **57**, 1497- 1514.

Knippertz, P., and H. Wernli, 2010: A Lagrangian climatology of tropical moisture exports to the Northern Hemispheric extratropics. *J. Clim*., **23**, 987-1003.

Large, W. G., and S. G. Yeager, 2009: The global climatology of an interannually varying air–sea flux data set. *Clim Dyn.,* **33**, 341–364.

Lenters, J. D., M. T. Coe, and J. A. Foley, 2000: Surface water balance of the continental United States, 1963-1995: Regional evaluation of a terrestrial biosphere model and the NCEP/NCAR reanalysis. *J. Geophy. Res.,* **105**, 22393-22425.

Lin, J., B. Mapes, M. Zhang, and M. Newman, 2004: Stratiform Precipitation, Vertical Heating Profiles, and the Madden–Julian Oscillation. *J. Atmos. Sci.*, **61**, 296–309.

Min, W., and S. Schubert, 1997: The climate signal in regional moisture fluxes: a comparison of three global data assimilation products. *J. Climate*, **10**, 2623-2642.

Mo, K. C., M. Chelliah, M. L. Carrera, R. W. Higgins, and W. Ebisuzaki, 2005: Atmospheric Moisture Transport over the United States and Mexico as Evaluated in the NCEP Regional Reanalysis. *J. Hydrometeor*. **6**, 710-728.

Mo, K., and R. W. Higgins, 1996: Large-scale atmospheric moisture transport as evaluated in the NCEP/NCAR and the NASA/DAO reanalyses. *J. Clim*., **8**, 1531-1545.

Neiman, P. J., F.M. Ralph, G.A. Wick, J. Lundquist, and M.D. Dettinger, 2008a: Meteorological characteristics and overland precipitation impacts of atmospheric rivers affecting the West Coast of North America based on eight years of SSM/I satellite observations. *J. Hydrometeor.*, **9**, 22-47.

Neiman, P. J., F. M. Ralph, G. A. Wick, Y.-H. Kuo, T.-K. Wee, Z. Ma, G. H. Taylor, and M. D. Dettinger, 2008b: Diagnosis of an intense atmospheric river impacting the Pacific Northwest: Storm summary and offshore vertical structure observed with COSMIC satellite retrievals. *Mon. Wea. Rev.*, **136**, 4398-4420.

Newman M., P. D. Sardeshmukh, and J. W. Bergman, 2000: An assessment of the NCEP, NASA and ECMWF reanalyses over the Tropical West Pacific warm pool. *Bull. Amer. Meteor. Soc.*, **81**, 41-48

Newman, M., P. D. Sardeshmukh, C. Penland, 2009: How Important Is Air–Sea Coupling in ENSO and MJO Evolution? *J. Climate*, **22**, 2958–2977.

Pauluis, O., T. Shaw, and F. Laliberté, 2011: A statistical generalization of the transformed Eulerian-mean circulation for an arbitrary vertical coordinate system. *J. Atmos. Sci.,* **68,** 1766-1783.

Peixoto, J. P., and A. H. Oort, 1992: Physics of Climate. Amer. Inst. Phys. 520 pp.

Pierrehumbert R.T., 1998: Lateral mixing as a source of subtropical water vapor. *Geophysical Research Letters,* **25**, 151-154.

Ralph, F. M., P. J. Neiman, and G. A. Wick, 2004: Satellite and CALJET aircraft observations of atmospheric rivers over the eastern North Pacific ocean during the winter of 1997/98. *Mon. Wea. Rev.*, **132**, 1721-1745.

Ralph, F. M., P. J., Neiman and R. Rotunno, 2005: Dropsonde observations in low-level jets over the Northeastern Pacific Ocean from CALJET-1998 and PACJET-2001: Mean vertical-profile and atmospheric-river characteristics. *Mon. Wea. Rev.,* **133**, 889-910.

Ralph, F. M., P. J. Neiman, G. N. Kiladis, K. Weickman, and D. W. Reynolds, 2011: A multi-scale observational case study of a Pacific atmospheric river exhibiting tropical-extratropical connections and a mesoscale frontal wave. *Mon. Wea. Rev.*, **139**, pp. 1169-1189, doi: 10.1175/2010MWR3596.1.

Roads, J. O., and A. Betts, 2000: NCEP-NCAR and ECMWF reanalysis surface water and energy budgets for the Mississippi river basin. *J. Hydrometeor.*, **1**, 88-94.

Roads, J. O., S.-C. Chen, A. K. Guetter, and K. P. Georgakakos, 1994: Large-scale aspects of the United States hydrologic cycle. *Bull. Amer. Meteor. Soc.*, **75**, 1589-1610.

Roads, J. O., M. Kanamitsu, and R. Stewart, 2002: CSE water and energy budgets in the NCEP–DOE Reanalysis II. *J. Hydrometeor*., **3**, 227–248.

Sardeshmukh, P.D., 1993: The baroclinic "chi" problem and its application to the diagnosis of atmospheric heating rates. *J. Atmos. Sci*, **50**, 1099-1112.

Sardeshmukh, P. D., and B. J. Hoskins, 1984: Spatial smoothing on the sphere. *Mon. Wea. Rev.,* **112**, 2524–2529.

Sardeshmukh, P. D., and B. L. Liebmann, 1993: An assessment of low-frequency variability in the tropics as indicated by some proxies of tropical convection. *J. Climate*, **6**, 569-575.

Sardeshmukh, P. D., M. Newman, and C. R. Winkler, 1999: Dynamically consistent estimates of diabatic heating. *Proceedings, 24th Annual Climate Diagnostics and Prediction Workshop*, Tucson, AZ, 172- 175

Schneider, T., P. A. O'Gorman, and X. J. Levine, 2010: Water vapor and the dynamics of climate changes. *Rev. Geophys.*, **48**, RG3001, doi:10.1029/2009RG000302.

Schneider, T., K. L. Smith, P. A. O'Gorman, and C. C. Walker, 2006: A climatology of tropospheric zonal-mean water vapor fields and fluxes in isentropic coordinates. *J. Climate*, **19**, 5918-5933.

Serreze, M, AP Barrett, AG Slater, RA Woodgate, K Aagaard, RB Lammers, M Steele, R Moritz, M Meredith, and C M Lee, 2006: The large-scale freshwater cycle of the Arctic. *J. Geophys. Res.*, **111**, C11010, doi:10.1029/2005JC003424

Serreze, M. C., A. P. Barrett, A. G. Slater, M. Steele, J. Zhang, and K. E. Trenberth, 2007: The large-scale energy budget of the Arctic. *J. Geophys. Res*., **112**, D11122, doi:10.1029/2006JD008230.

Shaw, T. A., and O. Pauluis, 2012: Tropical and subtropical meridional latent heat transports by disturbances to the zonal mean and their role in the general circulation. *J. Atmos. Sci.,* in press.

Simmons, A. J., J. M. Wallace, and G. W. Branstator, 1983: Barotropic wave propagation and instability, and atmospheric teleconnection patterns. *J. Atmos. Sci.,* **40,** 1363–1392.

Stohl, A., P. James, 2005: A Lagrangian Analysis of the Atmospheric Branch of the Global Water Cycle. Part II: Moisture Transports between Earth's Ocean Basins and River Catchments. *J. Hydrometeor*, **6**, 961–984, doi: 10.1175/JHM470.1.

Stohl, A., C. Forster, and H. Sodemann, 2008: Remote sources of water vapor forming precipitation on the Norwegian west coast at 60º N - a tale of hurricanes and an atmospheric river. *J. Geophys. Res.***113**, D05102, doi:10.1029/2007JD009006.

Trenberth, K. E., 1991: Climate diagnostics from global analyses: Conservation of mass in ECMWF analyses. *J. Climate*, **4**, 707-722.

Trenberth, K. E., 2011: Changes in precipitation with climate change. *Climate Research,* **47**, 123-138, doi:10.3354/cr00953.

Trenberth, K. E., and C. J. Guillemot, 1995: Evaluation of the global atmospheric moisture budget as seen from analyses. *J. Climate*, **8**, 2255-2272.

Trenberth, K. E., and C. J. Guillemot, 1998: Evaluation of the atmospheric moisture and hydrological cycle in the NCEP/NCAR reanalyses. *Clim. Dyn.*, **14**, 213-231.

Trenberth, K. E., L. Smith, T. Qian, A. Dai, and J. T. Fasullo, 2007: Estimates of the global water budget and its annual cycle using observational and model data. *J. Hydrometeor.*, **8**, 758-769.

Trenberth, K. E., J. T. Fasullo, and J. Mackaro, 2011: Atmospheric moisture transports from ocean to land and global energy flows in reanalyses. *J. Climate*, **24**, 4907-4924, doi: 10.1175/2011JCLI4171.1.

Tyrlis, E., and B. J. Hoskins, 2008: Aspects of a Northern Hemisphere atmospheric blocking climatology. *J. Atmos. Sci*., **65**, doi:10.1175/ 2007JAS2337.1.

van Loon, H., 1967: The half-yearly oscillation in middle and high southern latitudes and the coreless winter. *J. Atmos. Sci*. **24**, 472–486.

Wang, M. and J. Paegle, 1996: Impact of analysis uncertainty upon regional atmospheric moisture flux. *J. Geophy. Res.*, **101**, 7291-7303.

Whitaker, J.S., and P. D. Sardeshmukh, 1998: A linear theory of extratropical synoptic eddy statistics. *J. Atmos. Sci, 55, 237-258.*

Winkler, C. R., M. Newman, and P. D. Sardeshmukh, 2001: A linear model of wintertime low-frequency variability. Part I: Formulation and forecast skill. *J. Climate*, **14**, 4474-4494.

Yanai, M. S., Esbensen, S., and Chu, J. H. (1973). Determination of bulk properties of tropical cloud clusters from large-scale heat and moisture budgets. *J. Atmos. Sci.*, **30**, 611-627.

Yeh, P. J. F., M. Irizarry, and E. A. B. Eltahir, 1998: Hydroclimatology of Illinois: A comparison of monthly evapotranspiration estimates based on atmospheric water balance and soil water balance. *J. Geophys. Res*., **103**(D16), 19,823–19,837.

Zhu, Y., and R. E. Newell, 1998: A proposed algorithm for moisture fluxes from atmospheric rivers. *Mon. Wea. Rev.*, **126**, 725-735.

10. Figure Captions

Figure 1. Terms in the mean atmospheric water budget (2) for December-January-February (DJF) 1968-2007. Moisture flux divergence (shading) and moisture flux (vectors) for (a) total, (b) mean, (c) LF, and (d) synoptic terms from (4). Note that the moisture flux vectors in the top panels are scaled by 300 $kgm^{-1}s^{-1}$ and in the bottom panels by 30 $kgm^{-1}s^{-1}$; the moisture flux divergence contour level, however, is the same in all four panels.

Figure 2. Same as Fig. 1 but for June-July-August (JJA) 1968-2007.

Figure 3: Left panels: seasonal cycle of moisture transport from ocean to land in the a) Tropics, b) Northern hemisphere extratropics, and c) Southern hemisphere extratropics, where the tropical-extratropical boundaries are set as 20ºN and 20ºS. Right panels: seasonal cycle of moisture transport into the specified regions of d) North America, e) Europe (where the eastern boundary is set as 60ºE), and f) the Arctic (defined as the region north of 70ºN). The last pair of bars in each panel shows the annual mean terms. Mean, synoptic, and LF flux (transport) into each region is determined by the areal average of the flux convergence over each region. Precipitable water (w) tendency is also averaged in the region and multiplied by -1. Thus, the sign of all terms is chosen so that their sum (determined from the stacked bars on the left of each pair) is equal to $P - E$ also averaged in each region (blue bar on the right of each pair).

Figure 4: Seasonal cycle of vertically integrated, zonally averaged meridional moisture flux Q^y, for a) total flux, b) mean flux, c) LF flux, and d) synoptic flux. Contour interval

is 2.5 $kgm^{-1}s^{-1}$; positive is northward and negative is southward. e) Annual mean vertically integrated, zonally averaged meridional moisture flux Q^y.

Figure 5. Moisture flux divergence terms for DJF 1968-2007. Left panels: $<q\nabla\cdot\mathbf{v}>$. Right panels: $<\mathbf{v}\cdot\nabla q>$.

Figure 6. Moisture transport by bandpass anomalies for December-January-February (DJF) 1968-2007: flux divergence (shading) and corresponding moisture fluxes (vectors). Note that the moisture flux divergence contour level is reduced (relative to Fig. 1) to .125 mm/day and the moisture flux vectors are scaled by 10 $kgm^{-1}s^{-1}$.

Figure 7: Hovmuller of 4x daily total moisture flux Q (vectors, scaled by 600 $kgm^{-1}s^{-1}$) and column-integrated water vapor *w* (shading, contour interval 5 mm) at (a) 35ºN and (b) 45ºN for the winters DJF 2001-02 and 2002-03. Note that vectors show the local direction of the flux.

Figure 8: Same as Fig. 7a except for **Q** and *w* determined from data with synoptic components removed (left) or LF components removed (right).

Figure 9: DJF 4x daily moisture flux composited by different atmospheric river criteria: (a) ZN criterion, (b) N98 criterion, (c) "positive *w* plus positive v_{low}" criterion. Right hand panels (d-f) show the corresponding difference between total moisture flux (Fig. 1a) and composite flux on the left. Flux vectors are scaled by 300 $kgm^{-1}s^{-1}$. Shading in panels indicates the frequency of occurrence of (a-c) AR and (d-f) non AR conditions.

Figure 10. Moisture and meridional wind DJF climatology. (top) Mean DJF climate of precipitable water *w* (shading, contour interval 5 mm), variance of synoptic precipitable

water anomalies w'' (black, contour interval 10 mm^2), and variance of LF precipitable water anomalies w' (white, contour interval 10 mm^2). (bottom) Mean DJF climate of low-level (integrated between σ = .85 and 1) wind v_{low} (shading, contour interval 1 ms^{-1}), variance of synoptic low-level wind anomalies v''_{low} (black, contour interval 5 m^2s^{-2}), and variance of LF low-level wind anomalies v'_{low} (white, contour interval 5 m^2s^{-2}).

Figure 11. Schematics of extratropical (a) synoptic transport and (b) LF transport. a) "Lateral mixing" picture of synoptic moisture transport. At a given latitude indicated by the dashed line, a parcel advected by a poleward wind anomaly v'' (red arrow) will be coming from the equatorward side, so it will have moisture $w+\Delta w$, meaning that compared to the surrounding air $w''=\Delta w$ and there is poleward moisture flux $v''\Delta w$ (green arrow). Conversely, a parcel advected by an equatorward wind anomaly v'' (red arrow) will be coming from the poleward side, so its moisture is the same as the surrounding air, meaning that $w''=0$ and there is no moisture flux. b) Changes in the surface zonal winds (red lines) associated with anomalous deepening (left) or weakening (right) of the Aleutian low on LF time scales will drive anomalous surface evaporation (orange oval, indicating moisture source), and meridional wind anomalies will advect dry air equatorward and moist air poleward. This gives rise to moisture flux (green arrows) that is both northwestward and northeastward from the source region to the sinks (blue circles) since the anomalous moisture gradient is in the same direction as the wind anomaly. Since a LF anomaly of either sign will lead to the same pattern of moisture transport, on *average* this anomaly should contribute to mean transport.

Figure 12: Regression of u'_{low} , v'_{low} (indicated together by wind vectors, in ms^{-1}) and w' (indicated by color shading) on leading wintertime u'_{low} PC defined in (a) the Pacific sector and (c) the Atlantic sector. Composite of moisture flux (vectors) and moisture flux divergence (shaded) averaged over both +2 and -2 standard deviation events for (b) the Pacific sector and (d) the Atlantic sector; only values that are 95% significant (based on 1000 Monte Carlo simulations) are shown.

-

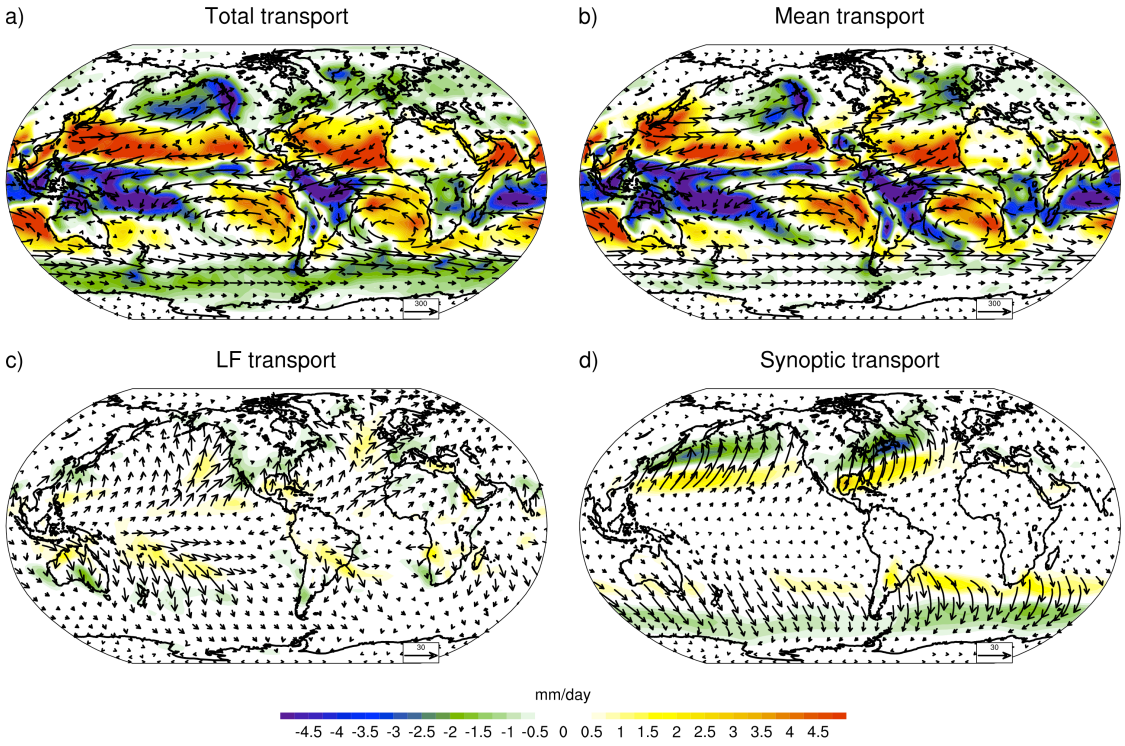

Figure 1. Terms in the mean atmospheric water budget (2) for December-January-February (DJF) 1968-2007. Moisture flux divergence (shading) and moisture flux (vectors) for (a) total, (b) mean, (c) LF, and (d) synoptic terms from (4). Note that the moisture flux vectors in the top panels are scaled by 300 $kgm^{-1}s^{-1}$ and in the bottom panels by 30 $kgm^{-1}s^{-1}$; the moisture flux divergence contour level, however, is the same in all four panels.

`

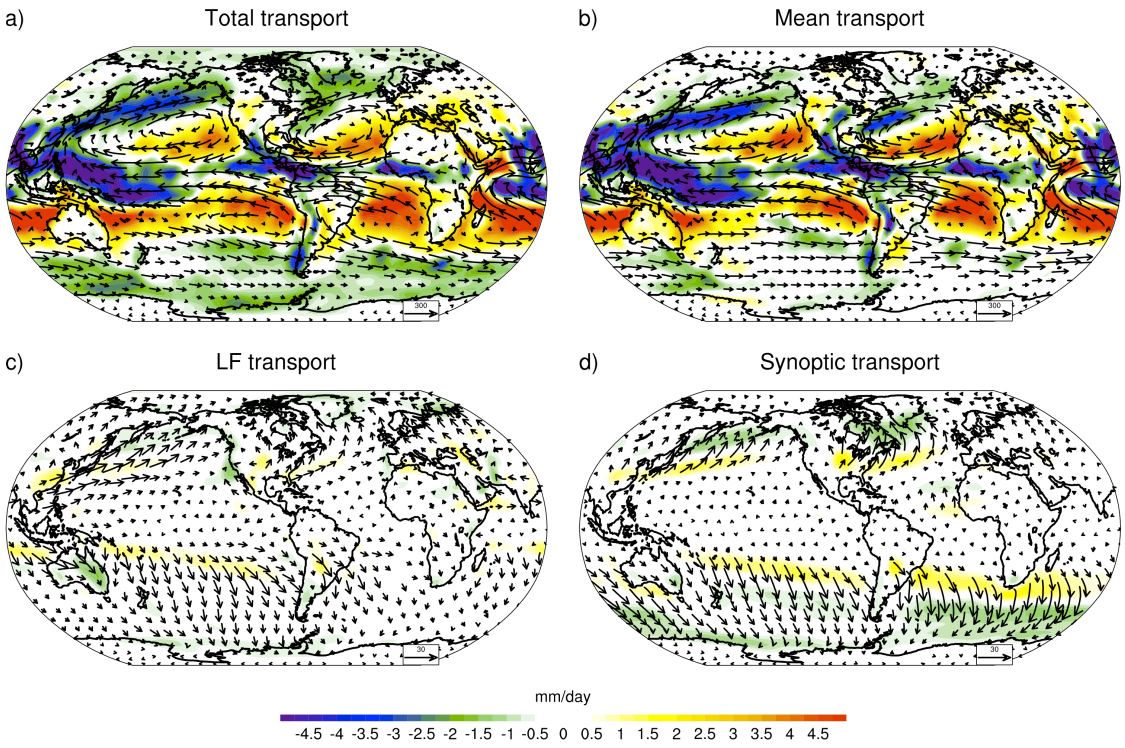

Figure 2. Same as Fig. 1 but for June-July-August (JJA) 1968-2007.

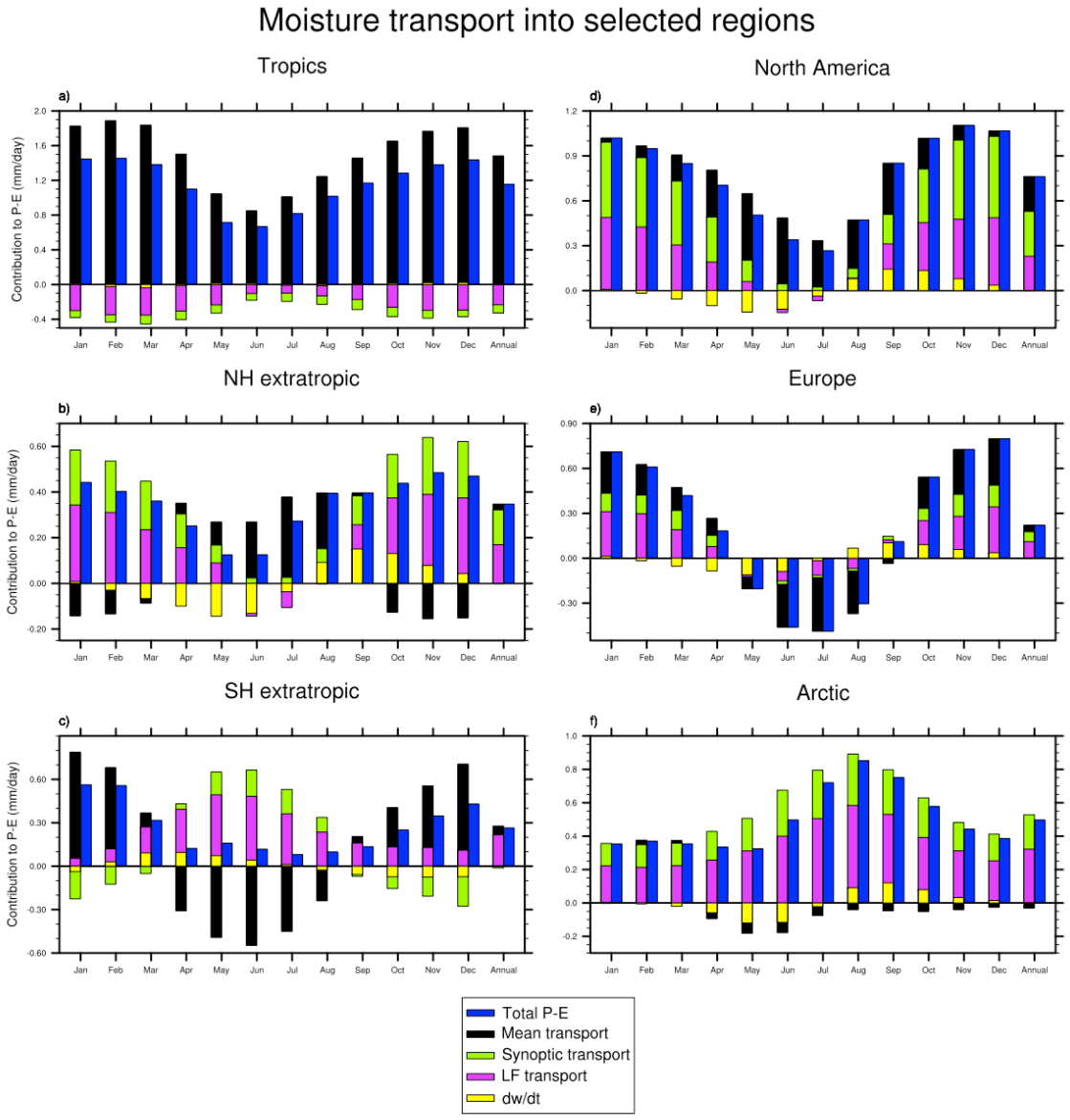

Figure 3: Left panels: seasonal cycle of moisture transport from ocean to land in the a) Tropics, b) Northern hemisphere extratropics, and c) Southern hemisphere extratropics, where the tropical-extratropical boundaries are set as 20ºN and 20ºS. Right panels: seasonal cycle of moisture transport into the specified regions of d) North America, e) Europe (where the eastern boundary is set as 60ºE), and f) the Arctic (defined as the region north of 70ºN). The last pair of bars in each panel shows the annual mean terms. Mean, synoptic, and LF flux (transport) into each region is determined by the areal average of the flux convergence over each region. Precipitable water (w) tendency is also averaged in the region and multiplied by -1. Thus, the sign of all terms is chosen so that their sum (determined from the stacked bars on the left of each pair) is equal to $P - E$ also averaged in each region (blue bar on the right of each pair).

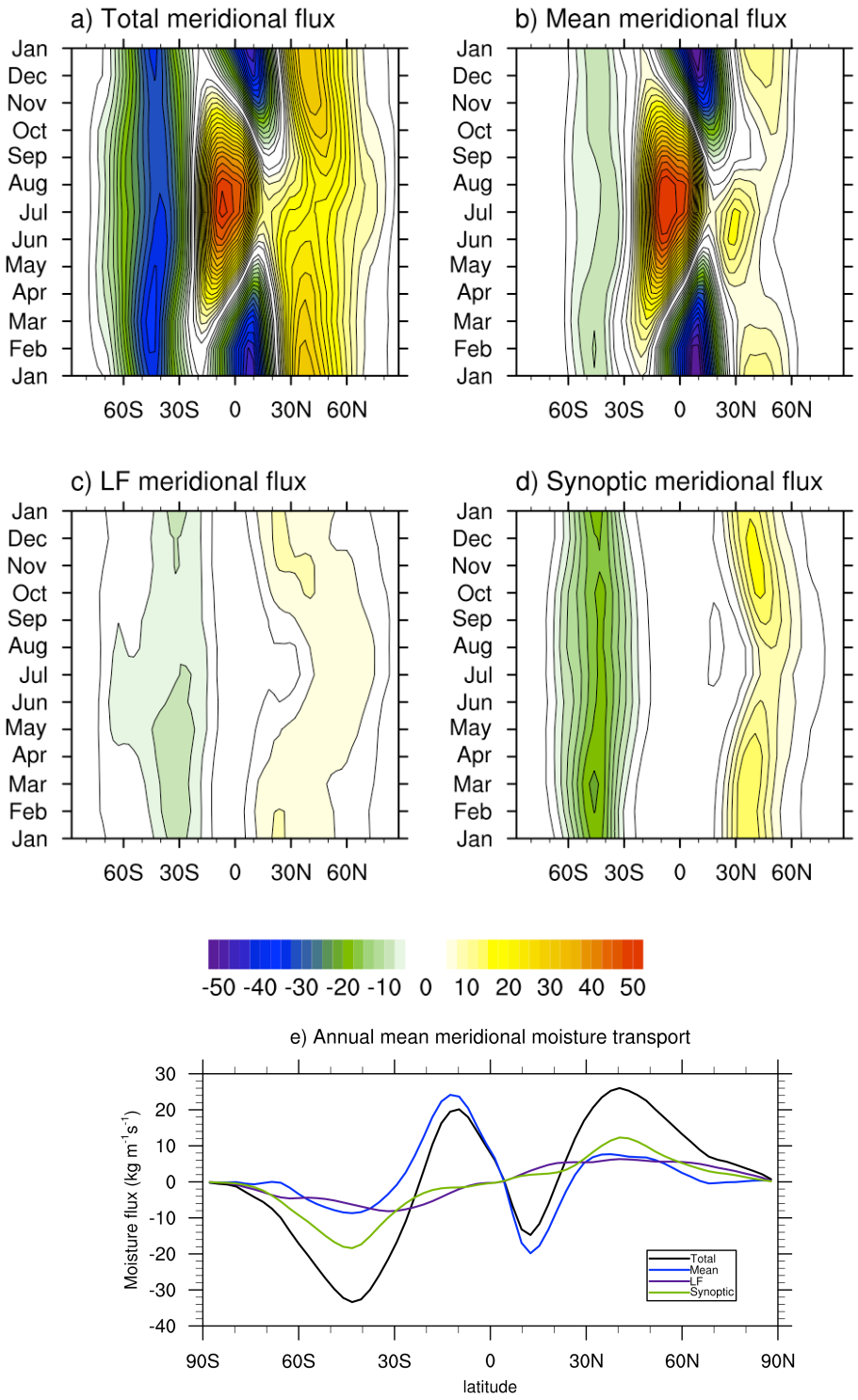

Figure 4: Seasonal cycle of vertically integrated, zonally averaged meridional moisture flux Q^y, for a) total flux, b) mean flux, c) LF flux, and d) synoptic flux. Contour interval is 2.5 $kgm^{-1}s^{-1}$; positive is northward and negative is southward. e) Annual mean vertically integrated, zonally averaged meridional moisture flux Q^y.

-

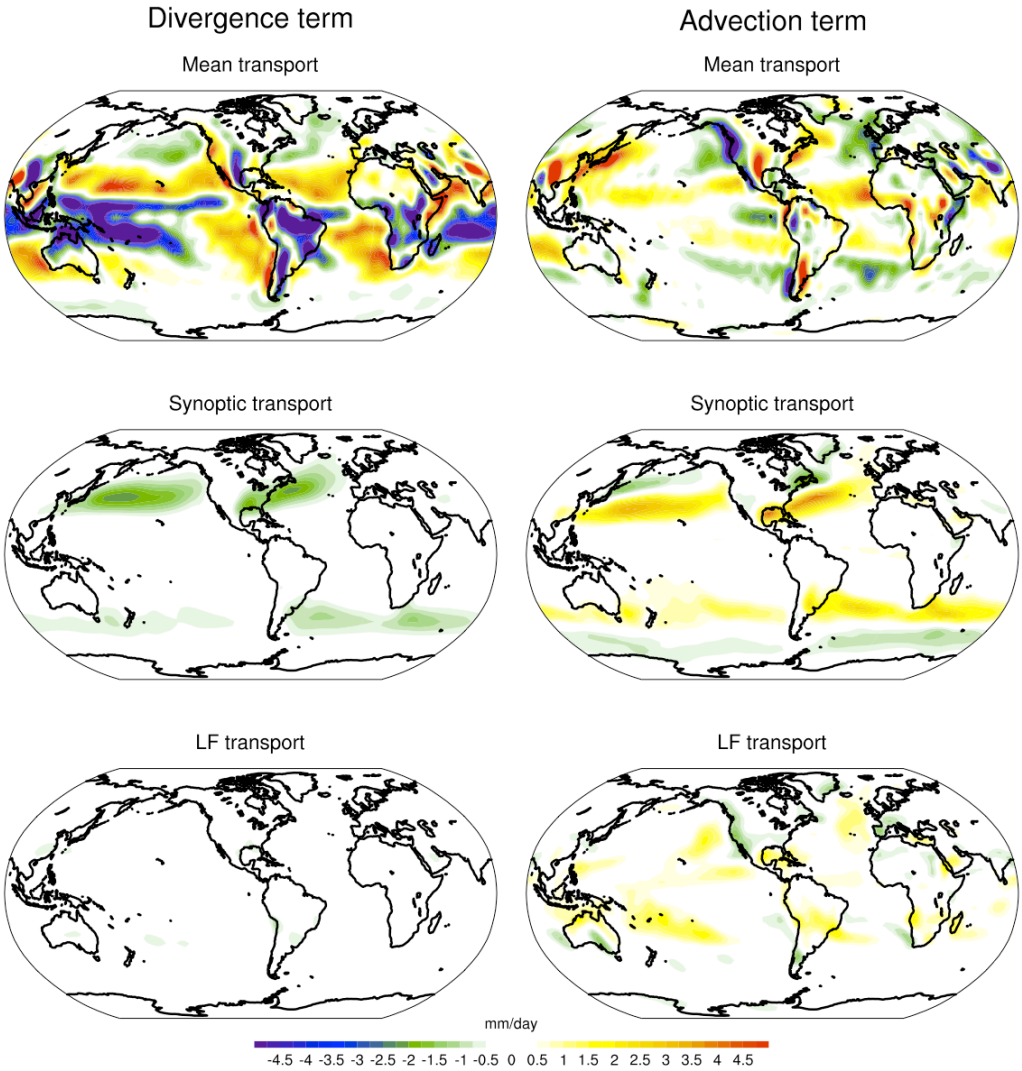

Figure 5. Moisture flux divergence terms for DJF 1968-2007. Left panels: $<q\nabla\cdot\mathbf{v}>$. Right panels: $<\mathbf{v}\cdot\nabla q>$.

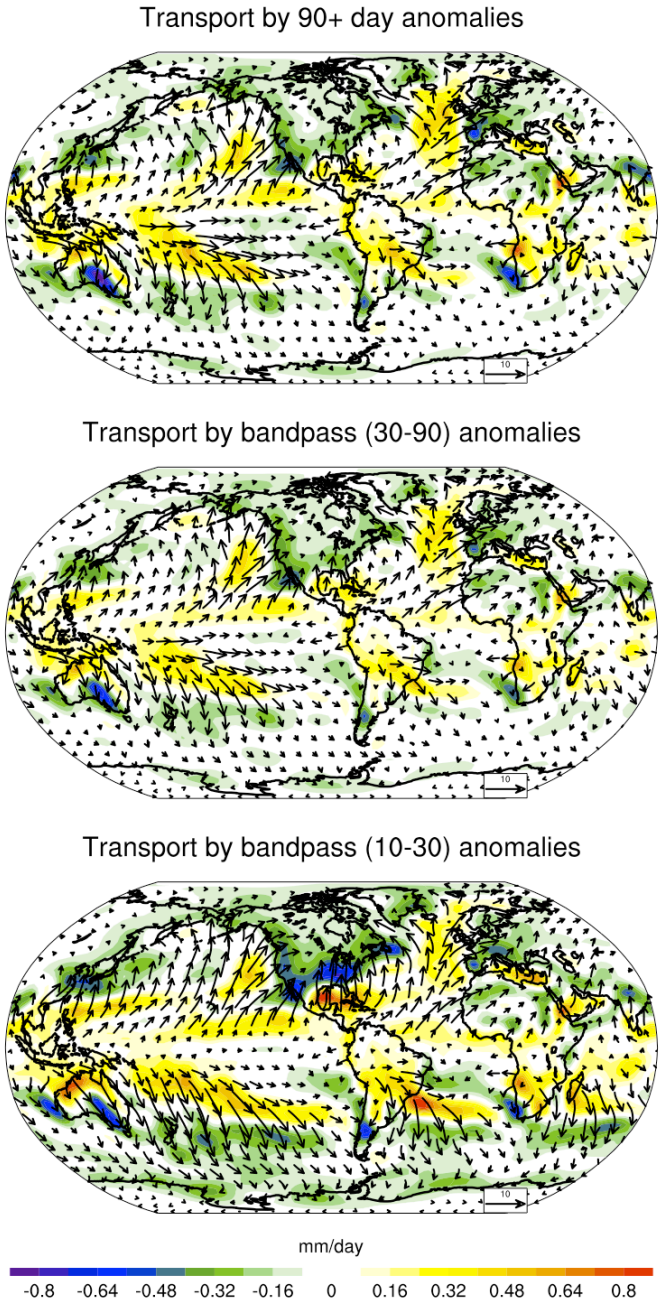

Figure 6. Moisture transport by bandpass anomalies for December-January-February (DJF) 1968-2007: flux divergence (shading) and corresponding moisture fluxes (vectors). Note that the moisture flux divergence contour level is reduced (relative to Fig. 1) to .125 mm/day and the moisture flux vectors are scaled by 10 $kgm^{-1}s^{-1}$.

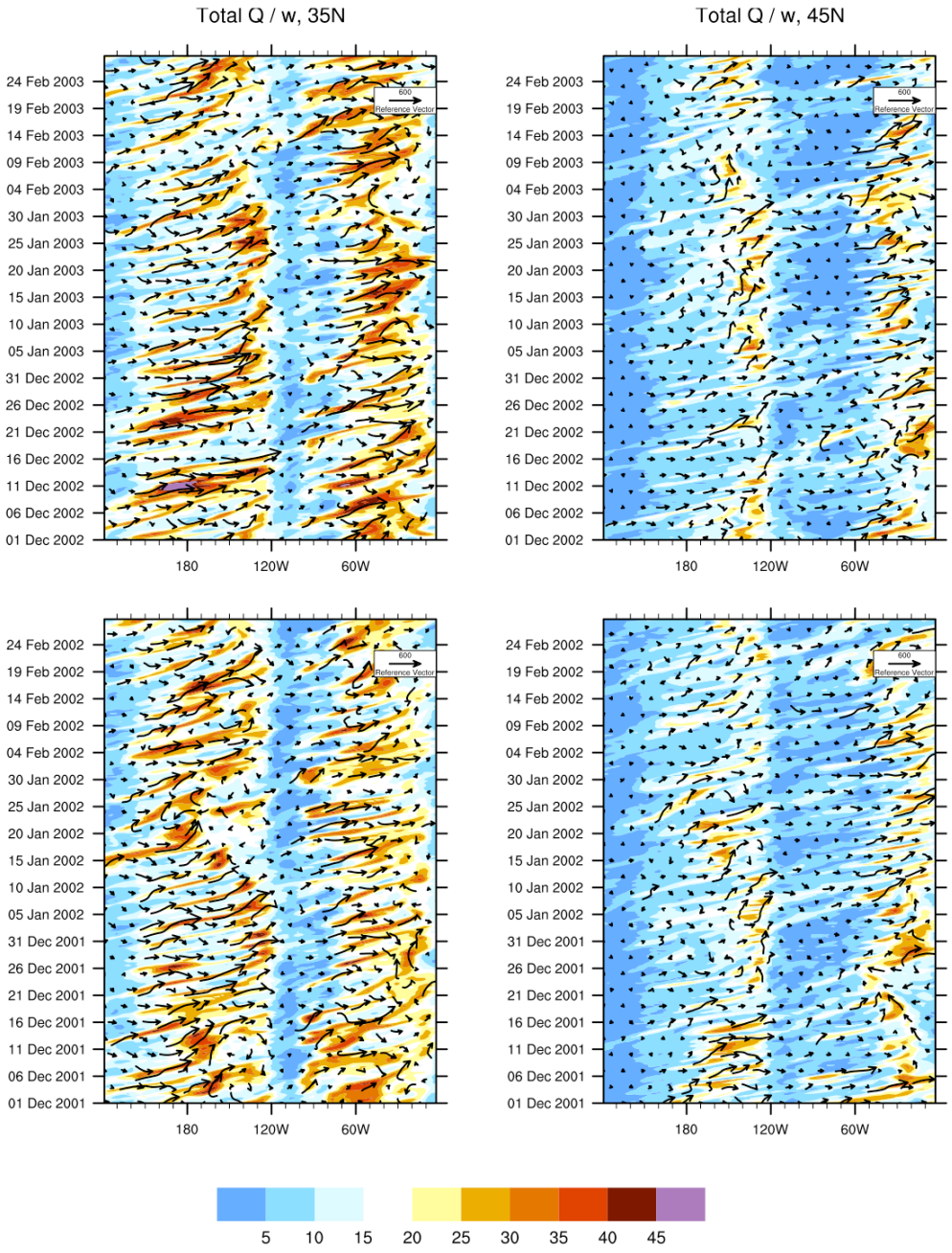

Figure 7: Hovmuller of 4x daily total moisture flux **Q** (vectors, scaled by 600 $kgm^{-1}s^{-1}$) and column-integrated water vapor *w* (shading, contour interval 5 mm) at (a) 35ºN and (b) 45ºN for the winters DJF 2001-02 and 2002-03. Note that vectors show the local direction of the flux.

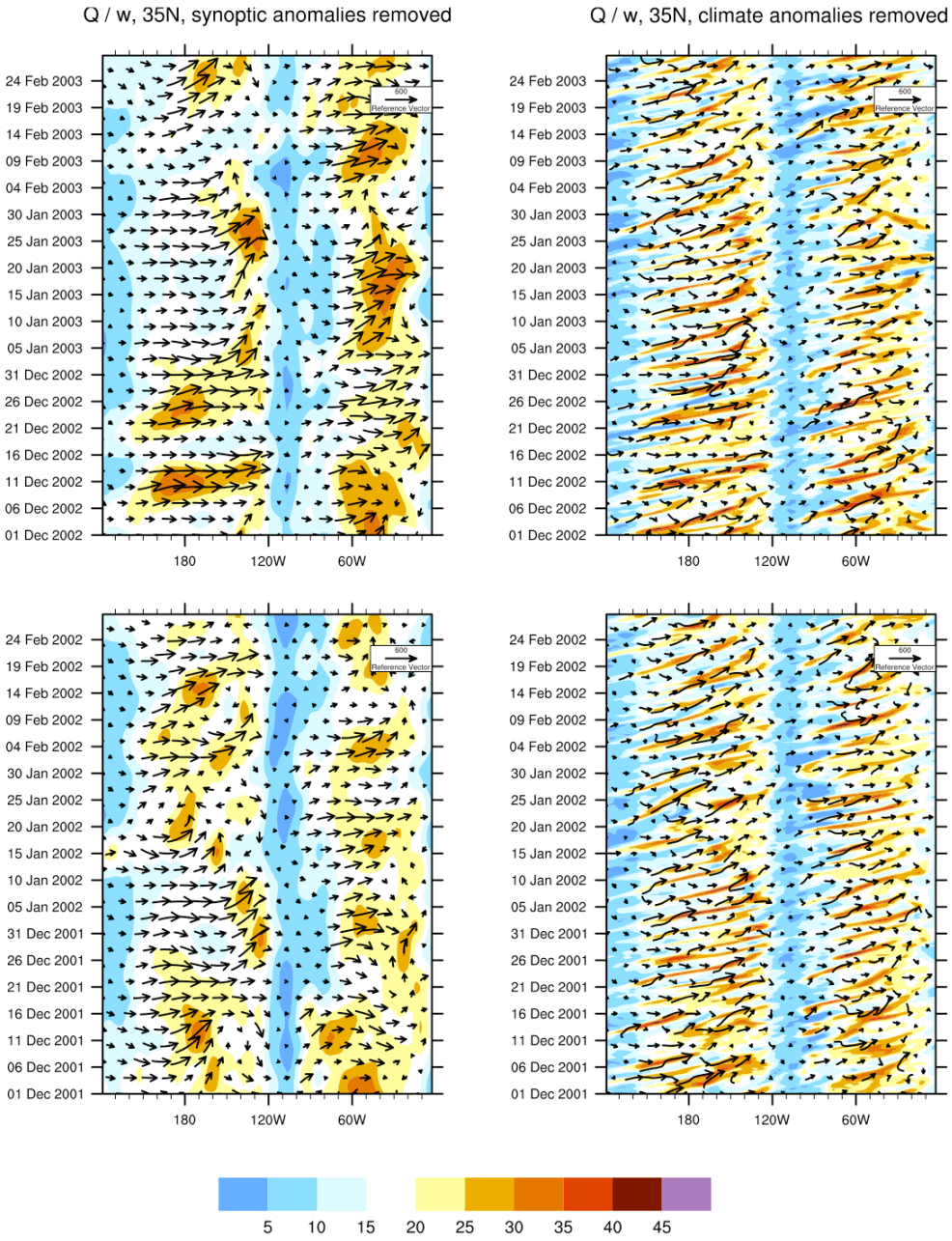

Figure 8: Same as Fig. 7a except for **Q** and *w* determined from data with synoptic components removed (left) or LF components removed (right).

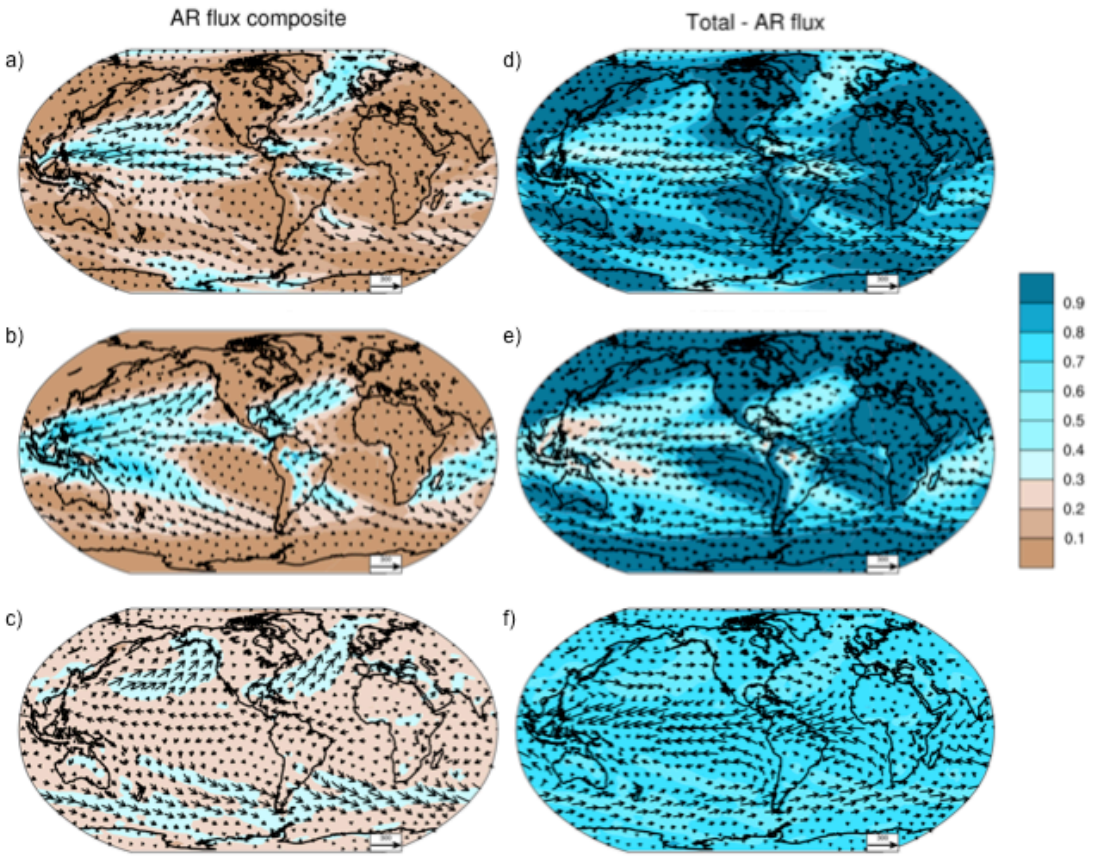

Figure 9: DJF 4x daily moisture flux composited by different atmospheric river criteria: (a) ZN criterion, (b) N98 criterion, (c) "positive *w* plus positive v_{low}" criterion. Right hand panels (d-f) show the corresponding difference between total moisture flux (Fig. 1a) and composite flux on the left. Flux vectors are scaled by 300 $kgm^{-1}s^{-1}$. Shading in panels indicates the frequency of occurrence of (a-c) AR and (d-f) non AR conditions.

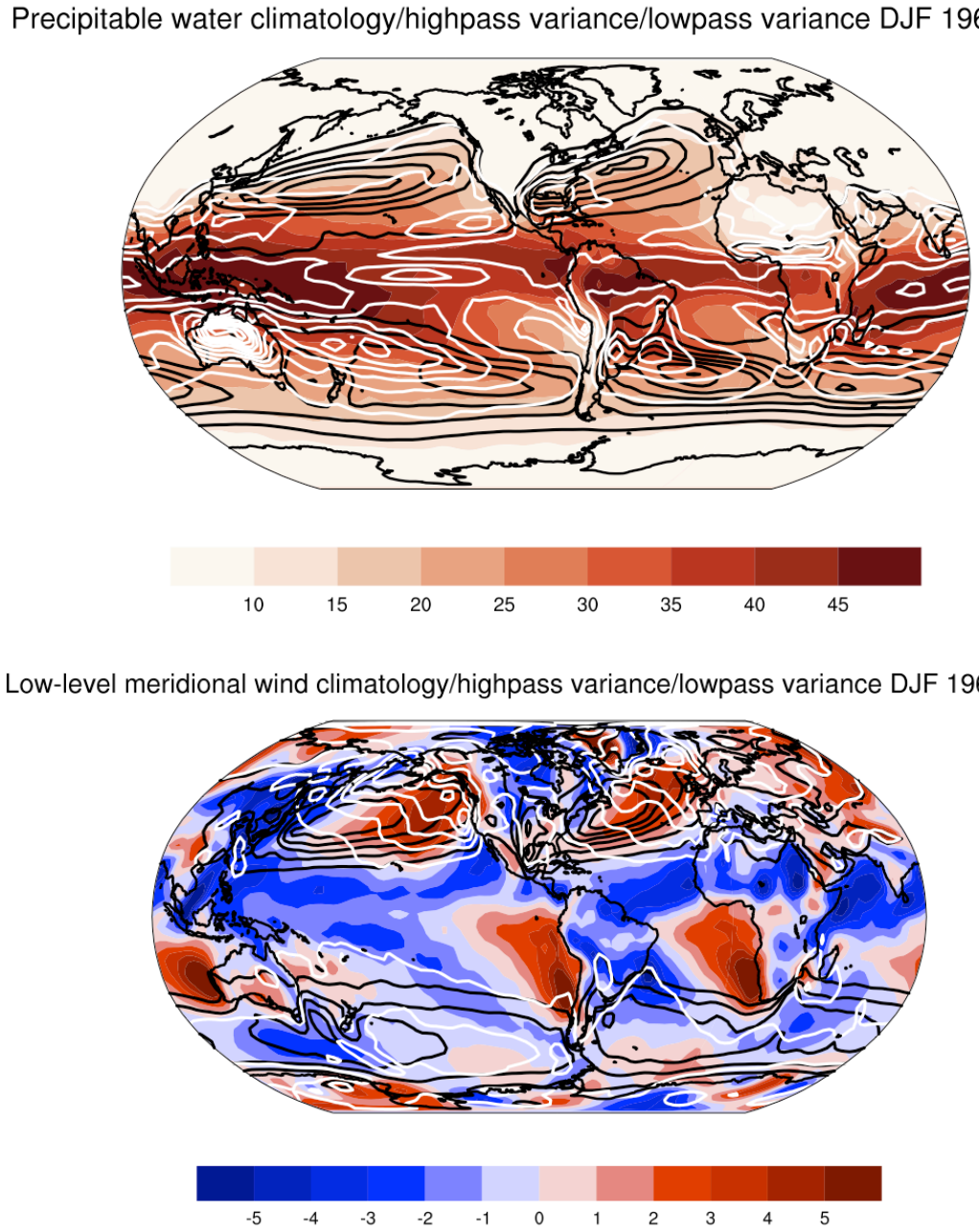

Figure 10. Moisture and meridional wind DJF climatology. (top) Mean DJF climate of precipitable water w (shading, contour interval 5 mm), variance of synoptic precipitable water anomalies w'' (black, contour interval 10 mm^2), and variance of LF precipitable water anomalies w' (white, contour interval 10 mm^2). (bottom) Mean DJF climate of low-level (integrated between $\sigma = .85$ and 1) wind v_{low} (shading, contour interval 1 ms^{-1}), variance of synoptic low-level wind anomalies v''_{low} (black, contour interval 5 m^2s^{-2}), and variance of LF low-level wind anomalies v'_{low} (white, contour interval 5 m^2s^{-2}).

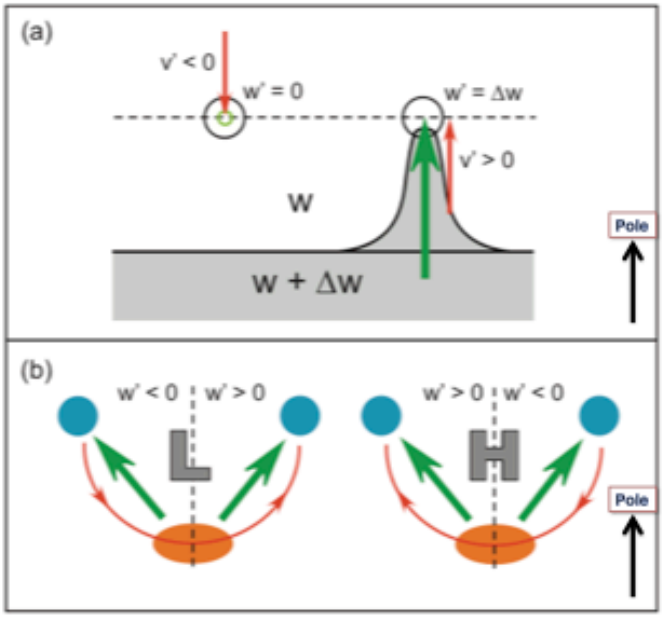

Figure 11. Schematics of extratropical (a) synoptic transport and (b) LF transport. a) ”Lateral mixing” picture of synoptic moisture transport. At a given latitude indicated by the dashed line, a parcel advected by a poleward wind anomaly *v*" (red arrow) will be coming from the equatorward side, so it will have moisture *w*+Δ*w*, meaning that compared to the surrounding air *w*"=Δ*w* and there is poleward moisture flux *v*"Δ*w* (green arrow). Conversely, a parcel advected by an equatorward wind anomaly *v*" (red arrow) will be coming from the poleward side, so its moisture is the same as the surrounding air, meaning that *w*"=0 and there is no moisture flux. b) Changes in the surface zonal winds (red lines) associated with anomalous deepening (left) or weakening (right) of the Aleutian low on LF time scales will drive anomalous surface evaporation (orange oval, indicating moisture source), and meridional wind anomalies will advect dry air equatorward and moist air poleward. This gives rise to moisture flux (green arrows) that is both northwestward and northeastward from the source region to the sinks (blue circles) since the anomalous moisture gradient is in the same direction as the wind anomaly. Since a LF anomaly of either sign will lead to the same pattern of moisture transport, on *average* this anomaly should contribute to mean transport.

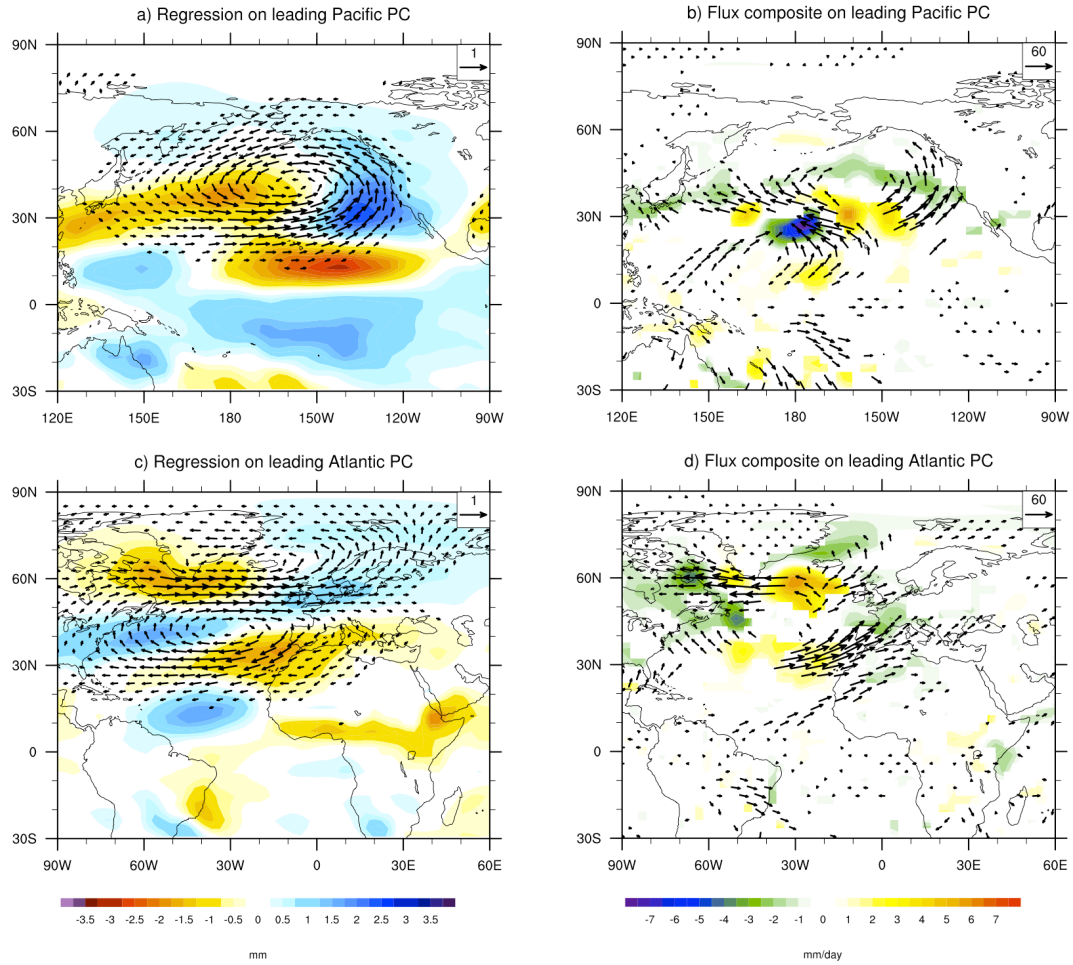

Figure 12: Regression of u'_{low} , v'_{low} (indicated together by wind vectors, in ms^{-1}) and w' (indicated by color shading) on leading wintertime u'_{low} PC (PC1) defined in (a) the Pacific sector and (c) the Atlantic sector. Composite of moisture flux (vectors) and moisture flux divergence (shaded) averaged over both +2 and -2 standard deviation values of PC1 for (b) the Pacific sector and (d) the Atlantic sector; only values that are 95% significant (based on 1000 Monte Carlo simulations) are shown.

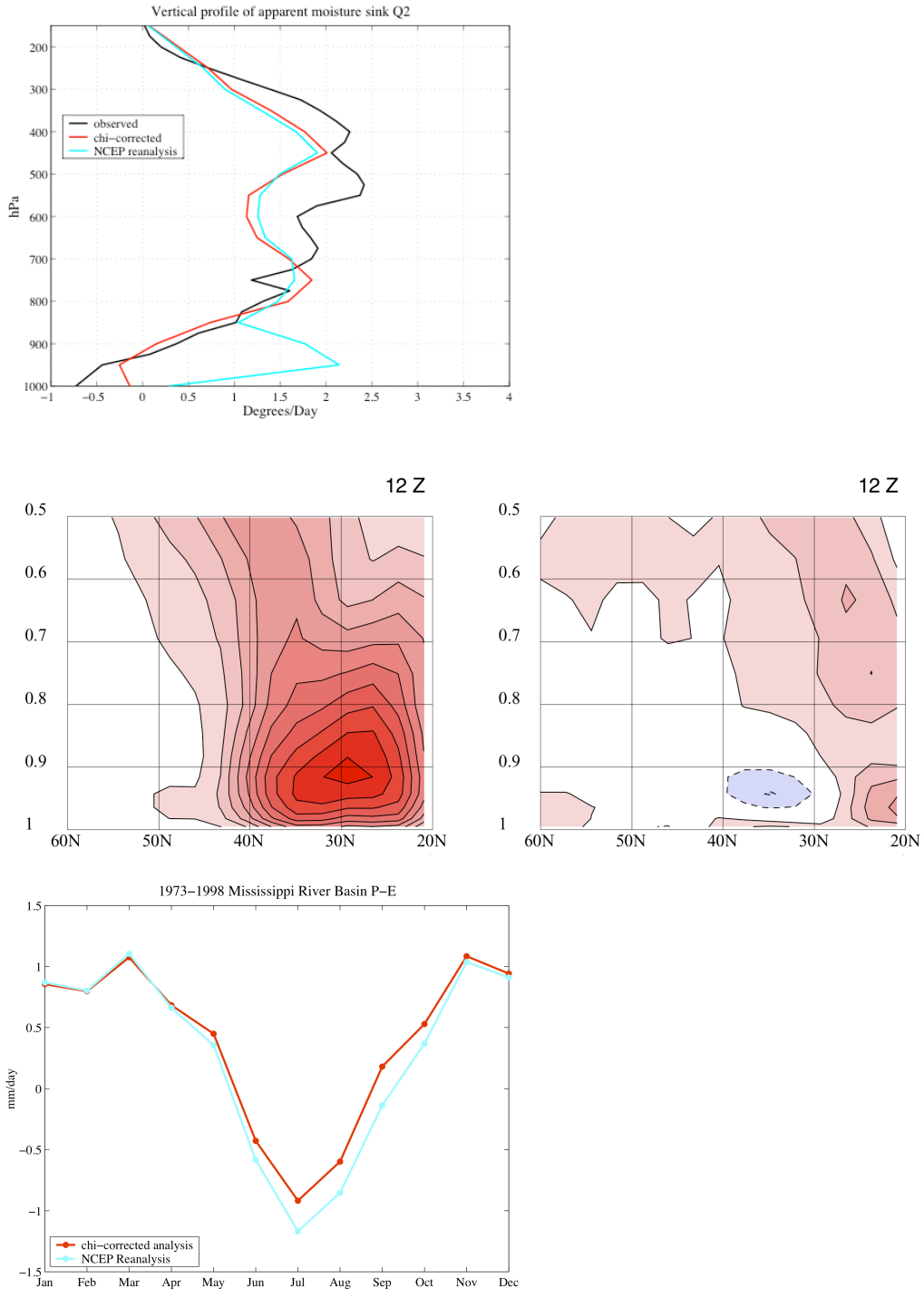

Figure A1. Comparison of chi-corrected and NCEP moisture flux divergences. top) Vertical profile of seasonally averaged (1 Nov 1992-28 Feb 1993) moisture sink Q2 from observations (black line), chi-corrected fields (red line) and NCEP Reanalysis (blue line). Units are K/day. Observations are taken from an updated version of Johnson and Lin's

(1997) dataset over the Intensive Flux Array (IFA) of COARE. NCEP and chi-corrected fields are measured at an analysis gridpoint (1.4S, 155E) near the center of the IFA region. middle) Latitude-sigma cross-sections of July 1993 monthly mean 12Z meridional wind speed, averaged between 95.5ºW-98.5ºW left: Chi-corrected total meridional wind. Contour interval 1.2 m/s; red shading indicates positive values and starts at 1.2 m/s. right: Difference fields (chi-corrected winds minus NCEP Reanalysis winds). Contour interval is 0.4 m/s; red shading indicates positive values and blue shading indicates negative values. Shading starts at + 0.4 m/s. Zero contour has been omitted for clarity. bottom) Seasonal cycle of P-E, area-averaged over a region similar to the Mississippi Basin region defined by Roads et al. (1994).